

Article

The Sedimentary Characteristics and Resource Potential of a Lacustrine Shallow-Water Delta on a Hanging-Wall Ramp in a Rift Basin: A Case Study from the Paleogene of the Raoyang Sag, Bohai Bay Basin, China

Lei Ye ^{1,*}, Xiaomin Zhu ^{1,*}, Nigel P. Mountney ² , Shuanghui Xie ¹, Renhao Zhang ³ and Luca Colombera ⁴

¹ College of Geosciences, China University of Petroleum, Beijing 102249, China; xsh_718@163.com

² Sedimentology Research Group, School of Earth and Environment, University of Leeds, Leeds LS2 9JT, UK; n.p.mountney@leeds.ac.uk

³ China JIKAN Research Institute of Engineering Investigations and Design, Co., Ltd., Xi'an 710000, China; 13683152485@163.com

⁴ Department of Earth and Environmental Sciences, University of Pavia, Via Ferrata 1, 27100 Pavia, Italy; luca.colombera@unipv.it

* Correspondence: yeleydia@163.com (L.Y.); xmzhu@cup.edu.cn (X.Z.)

Abstract: The hanging-wall ramps of rift basins are prone to the accumulation of large sedimentary bodies and are potential areas for the presence of large subsurface geological reservoir volumes. This paper comprehensively utilizes data from sedimentology, seismic reflection, geochemistry, and palynology to study the paleotopography, water conditions, paleoclimate, and sediment supply of the fourth member (Mbr 4) of the Shahejie Formation in the Raoyang Sag of the Bohai Bay Basin, China. The sedimentary characteristics, evolution, and preserved stratigraphic architectures of shallow-water deltaic successions are analyzed. Multiple indicators—such as sporopollen, ostracoda, fossil algae, major elements, and trace elements—suggest that when Mbr 4 was deposited, the climate became progressively more humid, and the lake underwent deepening followed by shallowing. During rift expansion, the lake level began to rise with supplied sediment progressively filling available accommodation; sand delivery to the inner delta front was higher than in other parts of the delta, and highly active distributary channels formed a reticular drainage network on the delta plain, which was conducive to the formation of sandstone up-dip pinch-out traps. In the post-rift period, the lake water level dropped, and the rate and volume of sediment supply decreased, leading to the formation of a stable dendritic network of distributary channels. At channel mouths, sediments were easily reworked into sandsheets. The distribution of sandstone and mudstone volumes is characterized by up-dip pinch-out traps and sandstone lens traps. The network of channel body elements of the shallow-water deltaic successions is expected to act as an effective carbon dioxide storage reservoir. This study reveals the influence of multiple factors on the sedimentary characteristics, evolution, and internal network of shallow-water deltas at different stages of rift basin evolution. This knowledge helps improve resource utilization and the sustainable development of comparable subsurface successions.



Academic Editor: Wei Jiang

Received: 3 November 2024

Revised: 17 December 2024

Accepted: 27 December 2024

Published: 30 December 2024

Citation: Ye, L.; Zhu, X.; Mountney, N.P.; Xie, S.; Zhang, R.; Colombera, L. The Sedimentary Characteristics and Resource Potential of a Lacustrine Shallow-Water Delta on a Hanging-Wall Ramp in a Rift Basin: A Case Study from the Paleogene of the Raoyang Sag, Bohai Bay Basin, China. *Sustainability* **2025**, *17*, 208. <https://doi.org/10.3390/su17010208>

Copyright: © 2024 by the authors. Licensee MDPI, Basel, Switzerland. This article is an open access article distributed under the terms and conditions of the Creative Commons Attribution (CC BY) license (<https://creativecommons.org/licenses/by/4.0/>).

Keywords: hanging-wall ramp; shallow-water delta; sedimentary environment; controlling factors; subsurface resource potential; Raoyang Sag

1. Introduction

Rift basins are noteworthy hydrocarbon-bearing basins: they account for about one-third of the giant oil fields worldwide [1]. Yet, in coming years and decades, basins of this type are likely to play an important role in the energy transition due to their potential to serve as large-scale permanent underground stores of carbon dioxide. In this regard, they are important for large-scale carbon capture and storage (CCS) projects to mitigate currently ongoing anthropogenic climate change.

The tectonic framework of rift basins generally allows the division of their physiography into basin margins (hanging-wall ramp and piedmont) and the basin floor. The basin margin is a favorable setting for the formation of coarse-grained fan deltas and Gilbert deltas, whereas the basin floor is conducive to the accumulation of turbidites [2–4]. However, these two types of physiographic domains are usually limited in size due to their topographic characteristics. A focus of the current research is the nature of sedimentary systems and their preserved successions accumulated upon low-gradient hanging-wall ramps of rift basins, which usually account for a large part of the basin area. The gentle terrain of this domain can accommodate a range of different types of fine-grained successions [5,6] and is notably conducive to the formation of large-scale shallow-water deltas, especially under conditions of sufficiently abundant sediment supply. These depositional systems have attracted the attention of sedimentologists, who have focused on their sedimentary characteristics [7–9], formation dynamics [10,11], sedimentary processes [12], and reservoir characterization [13], as well as on the responses of these sedimentary systems to sea-level, tectonic, or climatic changes [11,14,15]. Notably, large shallow-water deltaic depositional systems hosted on hanging-wall dip slopes of rifts in lacustrine basins exhibit considerable subsurface reservoir potential [7–9,11,16–20], including for CCS.

In relation to the tectonic evolutionary stages of basins, variations in tectonic activity affect the formation of sedimentary genetic units. Tectonic activity is typically relatively weak in the early stage of rift initiation and during the post-rift stage [21,22], and this may facilitate the formation of shallow-water deltas on hanging-wall slopes of lacustrine rift basins [15]. In this context, sandbodies usually develop on delta plains and delta fronts, often in the form of the infill of distributary channels. Under the influence of external controls and internal autogenic behaviors, complex channel morphodynamics may give rise to different topological relationships between the sandbodies, affecting their connectivity and their potential as reservoir volumes. Due to the gentle topography of the hanging wall and the potentially long distance of sediment transport, the rates of sediment input and lake level fluctuations can significantly affect sedimentary systems [9,23,24]. The rate of sediment supply is usually affected by factors such as tectonic activity, climate, the geology of the catchment area, the distance from the depocenter, and catchment size and relief [22,25,26]. Previous studies have made great progress in revealing relationships between sedimentary systems, the tectonic evolution of their host basin [22,27,28], and the reservoir characteristics of shallow-water deltas [7–15]. Yet, relatively few studies have been conducted on how the influence of geological controlling factors on sedimentary systems varies through different stages of rift evolution [29,30]. Therefore, within the scope of reservoir characterization, this paper comprehensively considers paleotopography, water conditions, paleoclimate, and sediment supply to try to reveal their influence on the sedimentary evolution and internal anatomy of shallow-water deltas through different stages of rift basin evolution, with consideration of their impact on subsurface resource potential, notably for CCS.

The Raoyang Sag is a significant target for hydrocarbon exploration in the Bohai Bay Basin, China. The Eocene Shahejie Formation is one of the primary oil and gas reservoirs in the Raoyang Sag. Extensive research has been conducted on the sequence stratigraphy,

provenance, and sedimentology of the Shahejie Formation [31]. Lacustrine shallow-water deltaic deposits are generally recognized in the fourth member (Mbr 4) of the Shahejie Formation of the Raoyang Sag. However, there remains controversy regarding the specific type of deltaic system embodied by these successions [32]. In addition, existing research suggests that (i) the climate during this period was relatively humid, with humidity increasing gradually through time, (ii) that the lake was shallow [33,34], and (iii) that sediment was mainly sourced from the Taihang range located to the west [35,36]. Yet, there remains a research gap regarding the impact of geological controls on changes in sedimentary environments through stratigraphy and across paleogeography.

The aim of this study is to elucidate the sedimentary characteristics, morphology, and controlling factors of lacustrine shallow-water deltaic deposits that accumulate on hanging-wall ramps of rift basins. The specific objectives are (1) to analyze the sedimentological characteristics of the succession and their spatial variability across the hanging-wall ramp of the Raoyang Sag; (2) to analyze stratigraphic variations that may reflect changes in climate, basin bathymetry, and sediment supply by integrating a variety of methods; and (3) to establish a depositional model for lacustrine shallow-water deltas installed on hanging-wall ramps of continental basins. The outcomes of this study can assist subsurface predictions applicable to the planning of programs of carbon capture and storage (CCS) in the Raoyang Sag and in other similar settings.

2. Geological Setting

The Raoyang Sag is a sub-basin of the Jizhong Depression of the Bohai Bay Basin, located in the middle of the Jizhong Depression, which is an NE-trending Cenozoic half-graben with a western topographic high and an eastern low. The northern part of the Raoyang Sag is linked to the Baxian Sag, whereas the southern part is adjacent to the Shenze Low Uplift. Its eastern part is separated by the Xianxian Uplift by boundary faults, whereas the western part lies adjacent to the Gaoyang Lower Uplift [37] (Figure 1A). The Raoyang Sag includes six secondary tectonic units, which are, respectively, the western slope zone, the western secondary trough zone, the central uplift zone, the central secondary trough zone, the eastern uplift, and the eastern secondary trough zone, from west to east (Figure 1B). The study area is located in the western slope zone, which is a large inherited dustpan-shaped hanging-wall ramp of the upper Proterozoic carbonate basement, covering an area of 2100 km² (Figure 1C).

In the Paleogene, the Raoyang Sag experienced four stages of tectonic evolution: (1) the early syn-rift stage (corresponding to the Kongdian Formation and the Mbr 1 of the Shahejie Formation), when the basin was rapidly filled such that the extant accommodation space was relatively limited; (2) the main syn-rift stage (corresponding to the Mbr 2 of the Shahejie Formation), when the maximum accommodation space was reached in the basin, leading to the accumulation of the most widespread and thickest part of the stratigraphy; (3) the late syn-rift stage (corresponding to the Mbr 3, the Mbr 4^L and the Mbr 4^M of the Shahejie Formation), when the basin underwent uplift; and (4) the post-rift stage (corresponding to the Mbr 4^U of the Shahejie Formation and the Dongying Formation) [32,35] (Figure 2).

During the Paleogene, the Kongdian Formation, Shahejie Formation, and Dongying Formation were deposited in this order in the Raoyang Sag. Among these units, the Shahejie Formation can be further divided into four members from base to top, labeled as Mbr 1 to Mbr 4. Among them, Mbr 1 consists primarily of variegated conglomerates, sandy conglomerates, red sandy mudstones, and gray mudstones with light gray gypsum mudstones and marls; Mbr 2 mainly comprises gray and dark gray mudstones, oil shales and black shales, and sand-prone conglomerates; Mbr 3 is mostly composed of red and light gray mudstones, sandstones, and sandy conglomerates; and Mbr 4 mainly consists of

red and grayish-green mudstones, oil shales, bioclastic limestones, gray sandstones, and sandy conglomerates.

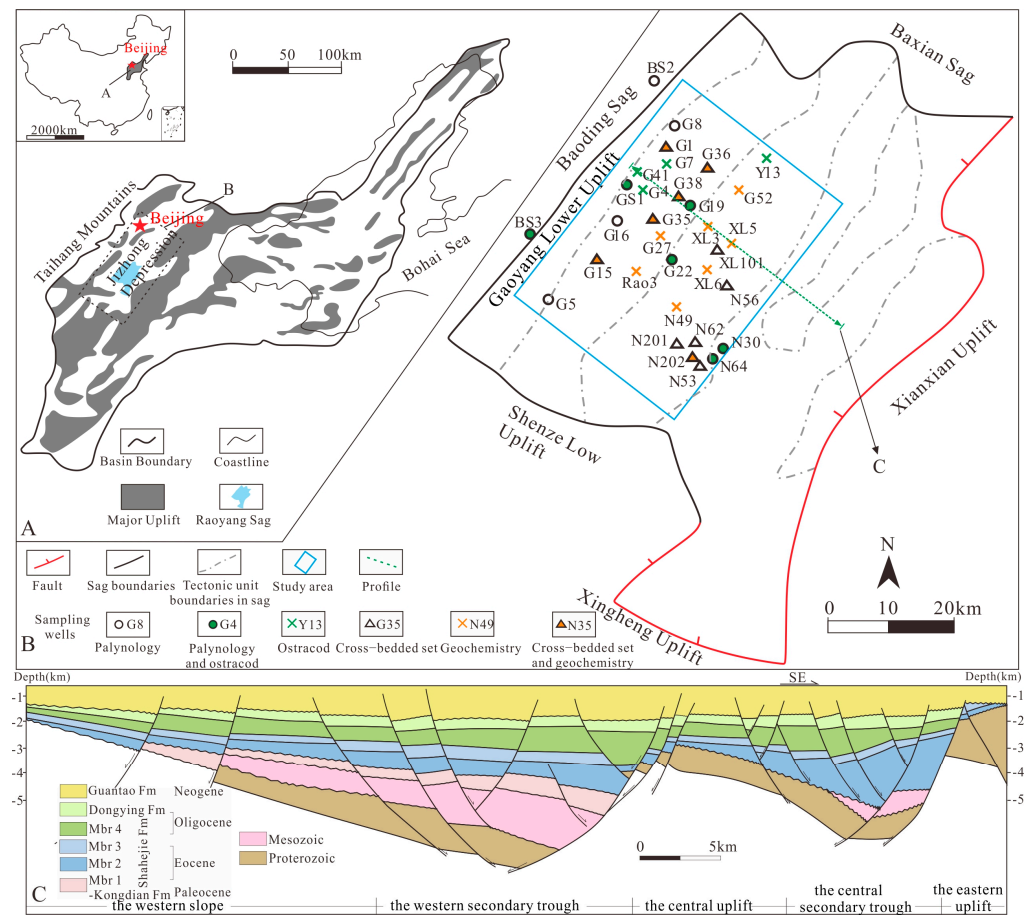


Figure 1. The geological setting and cross section of the Raoyang Sag. (A) The location of the Bohai Bay Basin in China. (B) The regional tectonic units of the Raoyang Sag and the location of the study area. (C) The regional stratigraphic cross section of the Raoyang Sag (the location of the cross section is shown in (B)).

The target interval of this study is the Mbr 4, whose top and base are defined by seismic reflections T_3 and T_{50} . Mbr 4 from base to top is further subdivided into three submembers, Mbr 4^L, Mbr 4^M, and Mbr 4^U, which are bounded by seismic reflections T_4 and T_{40} and have thicknesses in the ranges of 20–80 m, 50–150 m, and 130–540 m, respectively [35]. During the deposition of Mbr 4^L, the rift was uplifted, and a thin succession of gray sandstones with subordinate red mudstones was deposited. Subsequently, during the deposition of Mbr 4^M, the lake grew in size and the accommodation space increased rapidly. Gray mudstones, oil shales, bioclastic limestones, and nearshore sandstones of lacustrine origin were mainly deposited. Finally, during the time when Mbr 4^U was deposited, the lake area contracted, the accommodation space decreased, and a thick succession of deltaic deposits were accumulated; these consist of gray sandstones with carbonaceous mudstones, red and grayish-green mudstones, and sandy conglomerates with red mudstones [32,35] (Figure 2).

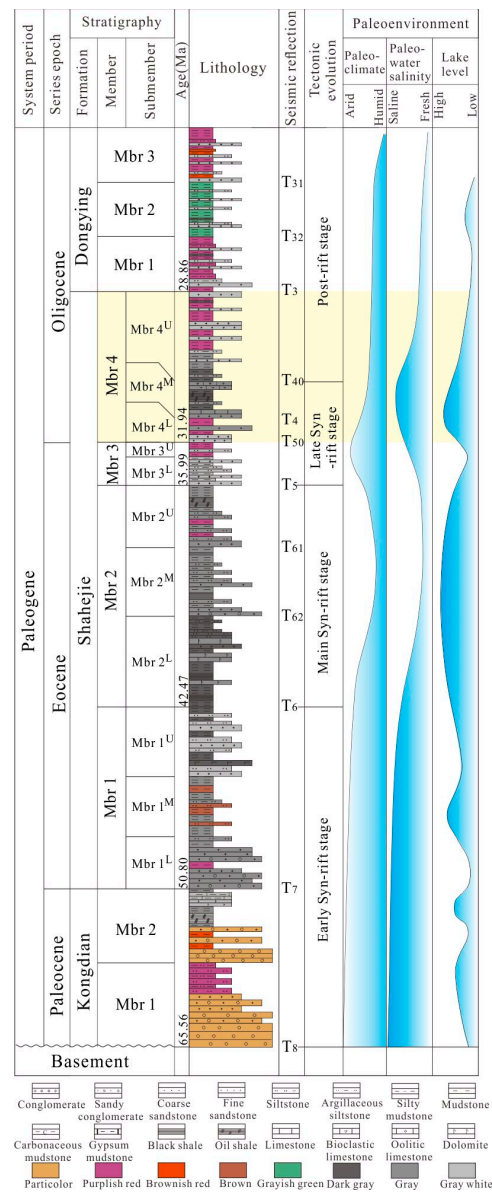


Figure 2. The paleogene stratigraphic column of the Raoyang Sag. The paleoenvironment curves refer to [38]. The target interval is the fourth member of the Shahejie Formation, highlighted in yellow. Mbr = Member, U = Upper, M = Middle, L = Lower.

3. Data and Methods

The datasets used in this study consist of 3D seismic reflection data, wireline logs, conventional cores, thin sections, grain size data, palynological data, and geochemical data. Analyses were undertaken to (1) identify sedimentological evidence of the evolution of lacustrine shallow-water deltas; (2) infer the factors that may have controlled the characteristics and distribution of sandbodies in the stratigraphy; and (3) establish a depositional model of lacustrine shallow-water deltas controlled by an interplay of factors during different rift stages.

3.1. Sedimentological Study

Based on the stratigraphic coverage and geographic distribution of the coreholes, 43 wells penetrating the Paleogene Shahejie Fm in the study area were selected; cores with a total length of 1260 m were observed and described. Facies associations were identified and classified by combining observations on lithology, thickness, sedimentary structures,

and mudstone color. Cored intervals are used for the calibration of wireline logs to guide facies recognition in areas lacking core data. Gamma-ray (GR), acoustic (DT), resistivity (RT), and spontaneous potential (SP) logs are used in this study. On a larger scale, the deltaic succession is studied by integrating well log and seismic data, with consideration of the distribution of sedimentary facies types.

3.2. Characterization of Delta Architecture and Channel Body Morphology

Making predictions of the presence and spatial distribution of sandbodies in shallow-water deltaic successions is especially challenging due to their limited thickness and the pronounced lateral variability in facies architecture and sandstone fractions that is typical of deltaic stratigraphies. Seismic data help address this by revealing the planform distribution and scale of seismically resolvable sedimentary bodies [39–42]. In the study area, post-stack three-dimensional seismic data are of high quality and wide extent (about 15,000 km²), covering most areas of the Raoyang Sag. The dominant frequency of the post-stack three-dimensional seismic data is 25 Hz, and the survey grid is 1 km × 1 km: this enables a morphological plan-view analysis of shallow-water deltaic architectures and sandbody distributions. Well and seismic data were calibrated using 43 well logs and synthetic seismograms (see well XL10 in Figure 3 as an example). To characterize the architecture of lacustrine shallow-water deltaic strata, this study selected T₃, T₄₀, and T₅₀ as marker layers to constrain stratal slices, extracting 50 stratal slices between each pair of successive marker layers. Attribute optimization was undertaken, revealing that the root mean square (RMS) amplitude attribute is the best proxy for lithology among the considered seismic attributes. Two sets of RMS attribute stratal slices (100 in total) were examined. The accuracy of the stratal slices was verified by lithology–impedance calibration. The planform architecture of the depositional system and the associated sandbody distribution were studied using the RMS attribute stratal slices. In addition, vertical seismic profiles were used to fully characterize the architecture of the lacustrine shallow-water deltaic succession.

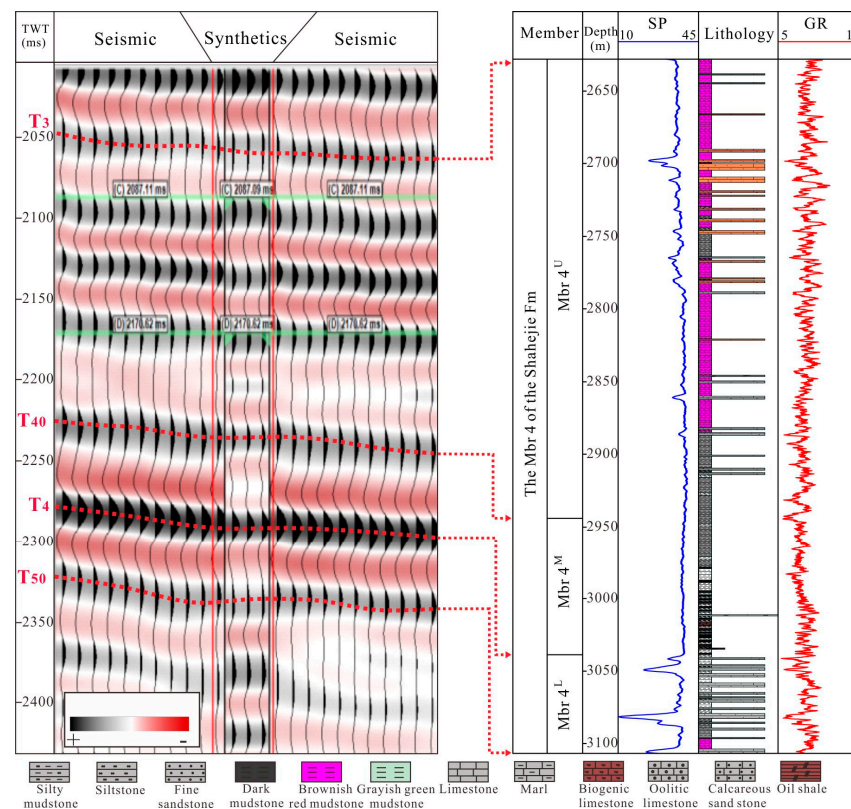


Figure 3. Seismic-well ties of well XL10. Synthetic seismograms were carried out on 43 wells.

3.3. Proxies for Paleoenvironmental Change

Different factors influence the development of deltas, including their paleotopography, climate, lake setting, and sediment supply. In this study, 56 mudstone samples from 13 wells were collected and sent to the Analysis and Test Research Center of Beijing Institute of Geology of Nuclear Industry. Axios-mAX wavelength dispersions X-ray fluorescence spectrometer (AB104L) and plasma mass spectrometer (NexION300D) were used to determine the contents of major elements and trace elements, respectively. In addition, the palynological data (83 mudstone samples from 9 wells) and ostracod data (64 mudstone samples from 10 wells) provided by Huabei Oilfield Branch Company of PetroChina were used for paleoclimate and paleobathymetry analysis. A total of 201 cross-bedded sets from 62 channel fills from 11 boreholes were measured to estimate sediment supply. The locations of sampling wells are shown in Figure 1B.

(1) Based on time–depth conversion and considering the relationship between porosity and depth, stratal thicknesses were decompacted so as to reconstruct the paleogeomorphology that existed before the deposition of Mbr 4 of the Shahejie Fm; paleotopographic gradients were measured. (2) Palynology and determining geochemical element ratios are common methods to characterize the paleoclimate. In this study, the considered paleoclimate proxies include Sr/Cu, Rb/Sr, Al₂O₃/MgO, and the distribution of different types of palynophytes [43–47]. (3) Some studies have shown that using paleontological markers with bathymetric significance to restore paleobathymetric depth is a reliable method [33,48–51]. Empirical formulas were used to infer paleobathymetry based on the contents of microalgae *Granulosus*, *Reticulosus*, and *Leiosphaeridia* and the diversity of ostracod fossil taxa (genera and species) [33,51,52]. In addition, water conditions can be indicated by geochemical indicators, and Ni/Co and δU were selected to reflect the paleoredox conditions in water [53–55], and Sr/Ba and Th/U were selected to reflect the paleosalinity [33,34]. (4) The thickness of sets of alluvial cross-bedded sets from distributary channel fills observed in core has been used to make empirical estimations of the bankfull depth and discharge for individual distributaries [56–60].

4. Results

4.1. Sedimentary Facies Belts of the Shallow-Water Delta

According to the color, facies characteristics, well log expression, and seismic response of different rock types, this study interpreted this succession as the preserved product of a lacustrine shallow-water deltaic depositional system, which was divided into three facies belts (Table 1, Figure 4): delta plain, delta front, and prodelta and offshore shallow lake. These three facies belts were further divided into eleven facies associations representing the deposits of subaerial distributary channels, floodplains, levees, crevasse splays, subaqueous distributary channels, interdistributary bays, subaqueous levees, mouth bars, delta front sandsheet, beach and bar, and prodelta and lacustrine mudstone.

Table 1. Sedimentary characteristics of facies belts and facies association of lacustrine shallow-water delta encountered in fourth member of Shahejie Formation, Raoyang Sag, Bohai Bay Basin.

Facies Belt	Facies Association	Thickness (m)	Grain Size Trend	Well Log Characteristics	Interpretation
Delta Plain (FB1: DP)	Subaerial distributary channel (FA1: DCH)	0.4–1.7	Irregular fining-upward trend	Medium-amplitude bell shape and box shape in GR logs	Scour surface indicating erosion of mouth bar or channel deposits by younger channel forms [61–63]
	Flood plain (FA2: FP)	0.2–2	None	High-amplitude linear shape in GR and SP logs	Brownish-red mudstones indicate oxidizing environment during deposition or burial; grayish-green mudstone indicates water-logged conditions, such as those existing on swamps in plains; siltstone and argillaceous siltstone may have been deposited by floods flowing into surrounding marshes
	Levee (FA3: LV)	0.4–0.7	Thin interbedded sandstone and mudstone	Medium-amplitude jagged bell shape	Common ripples and ripple cross-lamination in siltstones are formed under action of unidirectional flood flow; these are interpreted as levee deposits, which are commonly associated with distributary channels and mouth bar [64]
	Crevasse splay (FA4: CS)	0.3–1	Beds with irregular fining-upward trends	Isolated peak shape and funnel shape with high–medium amplitude	Observed fining-upward trend is interpreted as product of waning flow following channel breaches during floods
Delta front (FB2: DF)	Subaqueous distributary channel (FA5: SDC)	0.2–1.7	Irregular fining-upward trend	Medium-amplitude jagged bell and box shape in GR log	According to lithology, erosional character of surfaces, and dark gray color of mudstones, this deposit is interpreted as subaqueous distributary channel fill
	Interdistributary bay (FA6: IDB)	0.3–1.3	No systematic trend	A linear or microdentate signature with high amplitude in GR log	Highly bioturbated and burrowed, with wavy or lenticular bedding, and dark mudstones, this is interpreted as subaqueous low-energy environment
	Subaqueous levee (FA7: SLV)	0.4–0.8	Irregular fining-upward trend	Medium-high amplitude bell shape	Levee of possible subaqueous conditions in relation to finer grain size and darker color relative to deposits of FA3
	Mouth bar (FA8: MB)	0.4–0.6	Coarsening-upward trend	Funnel shape and box shape with medium amplitude	Mouth bar deposits, containing sporadic carbonaceous laminae deposited under low-energy conditions [65] Wave ripple marks indicate influence by lake processes; it often occurs in combination with deposits of subaqueous distributary channels, and its top is usually scoured by channel forms
Prodelta and offshore shallow lake (FB3: SL)	Sandsheet (FA9: SS)	0.1–0.5	Composite rhythm	Finger, funnel, and composite shape with medium amplitude	This is interpreted as product of reworking of subaqueous distributary channel and channel mouth deposits by waves and longshore currents
	Beach and bar (FA10: BB)	0.2–1	Composite rhythm, coarsening-upward trend	Finger, box, and funnel shape with low amplitude in GR log	Grain size characteristics indicate relatively strong hydrodynamic energy, possibly in relation to wave activity [66,67]
	Prodelta and lacustrine mudstone (FA11: LM)	1–3	No systematic trend	Linear or slightly jagged shape with very high amplitude in GR log	Quiet water, reducing lake environment

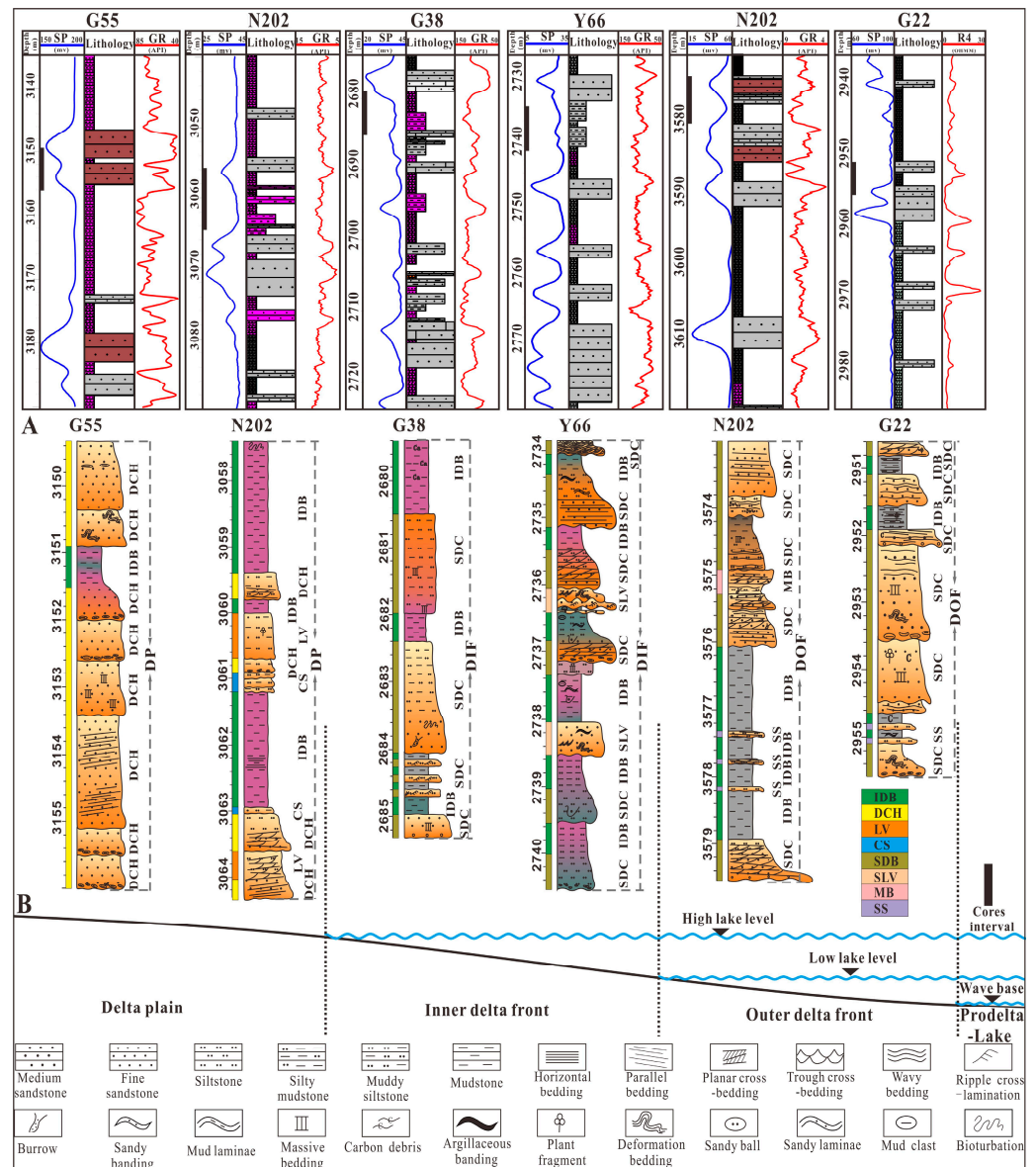


Figure 4. Sedimentary successions of the fourth member of the Shahejie Formation. The facies characteristics (A) and dip profile of subenvironments (B) of the shallow-water deltas. Refer to Table 1 for codes denoting facies associations.

4.1.1. Delta Plain (FB1)

The shallow-water delta plain is the domain of the delta located above the lake level and transitioning from upstream alluvial plains or valleys. The delta plain usually exhibits sedimentary characteristics that are similar to those of fluvial successions. This facies belt is characterized by large sections of purplish red mudstone embedded with fine sandstone and siltstone displaying fining-upward trends, large bed thicknesses, and channelization (Figure 4A). It mainly consists of subaerial distributary channel (FA1), flood plain (FA2), levee (FA3), and crevasse splay (FA4) facies associations; FA1 and FA2 are the most common ones. All of these facies associations indicate that the delta plain facies belt is relatively proximal and dominated by energetic processes. Delta plain strata in the study area are mostly observed in the upper part of Mbr 4^U of the Shahejie Fm.

4.1.2. Delta Front (FB2)

The delta front is the underwater domain of the delta located just offshore of the lake shoreline [68]. Lake water-level fluctuations over gentle gradients result in a differentiation of the delta front into inner and outer front regions. The inner delta front is the bathymetric part between the low and high water levels, which may be periodically exposed (Figure 4B). The permanently submerged portion of the delta front is termed the outer front. The facies belt consists of the subaqueous distributary channel (FA5), interdistributary bay (FA6), subaqueous levee (FA7), mouth bar (FA8), and sandsheet (FA9) facies associations. Although subaqueous distributary channels and interdistributary bays are developed in both the inner and outer delta front, the interdistributary bays in the inner delta front are dominated by brownish red, gray, and grayish green mudstones (Figure 4A), and the lateral continuity of the channels is larger. In contrast, the interdistributary bays in the outer delta front lack brownish red mudstones [9]. The shallow-water delta front in the study area is mainly developed at the bottom of Mbr 4^U and Mbr 4^L of the Shahejie Fm.

4.1.3. Prodelta and Offshore Shallow Lake (FB3)

The prodelta refers to the part of the delta slope located below the typical wave base (Figure 4B). Due to its distality relative to sediment entry points, it is dominated by deposition via suspension settling and is characterized by thick mudstone or heterolithic strata (Figure 4A). These mud-prone deposits are generally difficult to distinguish from lacustrine mudstones. Therefore, this study groups prodelta and offshore shallow-lake deposits into a single facies belt. In Mbr 4^M of the Shahejie Fm in the study area, this facies belt comprises nearshore beach and bar deposits and mudstones of the prodelta and offshore shallow lake.

4.2. Temporal and Spatial Evolution of the Shallow-Water Delta

4.2.1. Stratigraphic Changes and Delta Evolution

The seismic expression of shallow-water deltas was considered. In the Mbr 4^U interval, a seismic section oriented along the depositional dip shows multiple sets of imbricate seismic reflections with intermediate seismic amplitude and moderate continuity (Figure 5A,B). The deltaic edifices do not demonstrate well-developed sigmoidal clinoforms; this is interpreted as the expression of deltas that formed in a basin with limited bathymetry. As such, compared with the typical Gilbert deltas, deltas of this type have smaller clinoform gradients (1.43–2.17°) and a longer progradation distance (20 km). The slope clinoforms transition towards the basin into subparallel reflectors with high continuity and strong amplitude. The deltaic clinoforms downlap onto the base of Mbr 4^U of the Shahejie Fm interval (surface T₄₀) and show prominent progradational geometries. Thanks to core and well log control at well G104, which passes through the seismic profile, a coarsening-upward succession is recognized, paralleled by a change in mudstone color from gray to grayish green and to brownish red, and by a variation in wireline log profiles from funnel-shaped (interpreted as mouth bar deposits) to bell-shaped and box-shaped profiles (interpreted as distributary channel deposits) (Figure 5C). These observations indicate progressive shallowing of the sedimentary environment in relation to delta progradation.

In members Mbr 4^M and Mbr 4^L of the Shahejie Fm, sub-parallel seismic reflections with medium-strong amplitude and high continuity are observed. However, due to the limited thickness of the stratal packages relative to the vertical resolution of the seismic data, internal architectures are not revealed in detail. In well G104, however, it can be seen that the mudstone content gradually increases in this unit, that the mudstone color varies gradually from brownish red to gray, and that bioclastic limestone appears in the upper part. The wireline-log curves also change from bell-shaped and box-shaped (interpreted

as distributary channel elements) to funnel-shaped and compound profiles (interpreted as mouth bar elements and beach and bars). Thus, the sedimentary environment changed from subaerial to subaqueous under conditions of delta retrogradation.

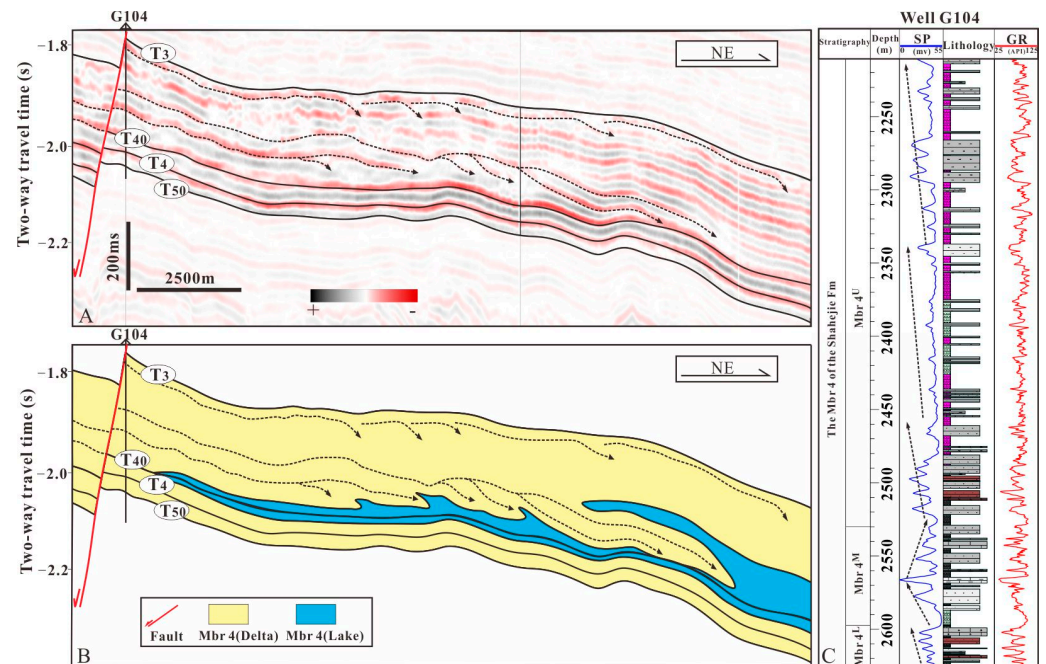


Figure 5. The imbricate seismic reflection characteristics of lacustrine shallow-water deltas of the fourth member of the Shahejie Formation. (A) The seismic profile along depositional dip. The dotted arrows indicate imbricated seismic reflections. (B) The seismic interpretation of the seismic profile in Figure 5A. (C) The sedimentary characteristics and interpretation of well G104. The dotted arrows indicate stratal geometries.

4.2.2. Planform Morphology of Deltaic Sandbodies

Shallow-water deltas mainly developed in members Mbr 4^U and Mbr 4^L of the Shahejie Fm, whereas Mbr 4^M was dominated by lacustrine deposition. Thus, in order to study the characteristics of shallow-water deltas, a set of RMS amplitude stratal slices were extracted for Mbr 4^U and Mbr 4^L of the Shahejie Fm. The RMS amplitude stratal slices were interpreted in terms of lithology. Seismic impedance is the highest for sandstone, followed by silty mudstone, argillaceous siltstone, and mudstone, which has the lowest impedance [15,36]. Therefore, seismic impedance has been considered as a lithological proxy (Figure 6A), calibrated with well log and core data. In the presented RMS amplitude stratal slices, high RMS amplitudes (9000–14,000 readings) reflect sand-prone units, low RMS amplitudes (0–5000 readings) reflect mud-prone units, and intermediate RMS amplitudes (5000–9000 readings) reflect heterolithic units.

RMS amplitude stratal slice Ss49 (Figure 6B), extracted from Mbr 4^U of the Shahejie Fm, is interpreted as exhibiting three distinct shallow-water deltas with generally lobate planforms. Mud-prone regions interpreted as interdistributary-bay deposits are common. Features interpreted as distributary channel fills demonstrate a dendritic pattern and generally low sinuosity. The geometries of the channel bodies are indicative of channels that had restricted lateral mobility and limited connections in relation to mutual confluences or channel reoccupations following avulsion. The width of the imaged channel bodies ranges from 292 to 1110 m, and their longitudinal extension is usually between 17 and 22 km. Bifurcating subaqueous distributary channels and outer delta front sandsheets are recognized features. The shallow-water deltas cover an area of 984 km². High RMS amplitude domains, which are sandstone dominated, cover a large area, especially in the central

and southern parts of the study area. To the south, in proximity of wells G28 and N35, northeast- and northwest-trending high-RMS-amplitude elongated domains are interpreted as sandbodies deposited in subaqueous distributary channels located on the inner delta front, whereas intermediate–low-RMS-amplitude regions are interpreted as mud-prone interdistributary-bay fills (Figure 6C). The well log profiles of wells G28, G29, and G22 support the interpreted distribution of sand-prone units on Ss49, and the interpretation of some of these deposits support the infill of subaqueous distributary channels. Well G104 intersects mud-prone units, whose well log profiles are compatible with an interpretation as interdistributary-bay fills (Figure 6D). In the area near wells G22 and XL4, the stratal slice is mainly characterized by NW-trending high-RMS-amplitude domains that take the form of coalescing lobes; these are interpreted as deposits associated with a network of subaqueous distributary channels in the distal outer delta front, where sandsheets developed due to wave reworking. This sand-prone unit transitioned to a region with intermediate–low-RMS-amplitude expression to the northeast, around well XL105; this is interpreted as an area dominated by shallow-lake mudstones and a beach bar. To the north, around wells Y60 and Y51, a small region with a high RMS amplitude character is seen, which takes the form of elongated domains trending northeastward. This is surrounded by a large area dominated by intermediate RMS amplitudes, interpreted as heterolithic delta front deposits, in part related to sedimentation by subaqueous distributary channels.

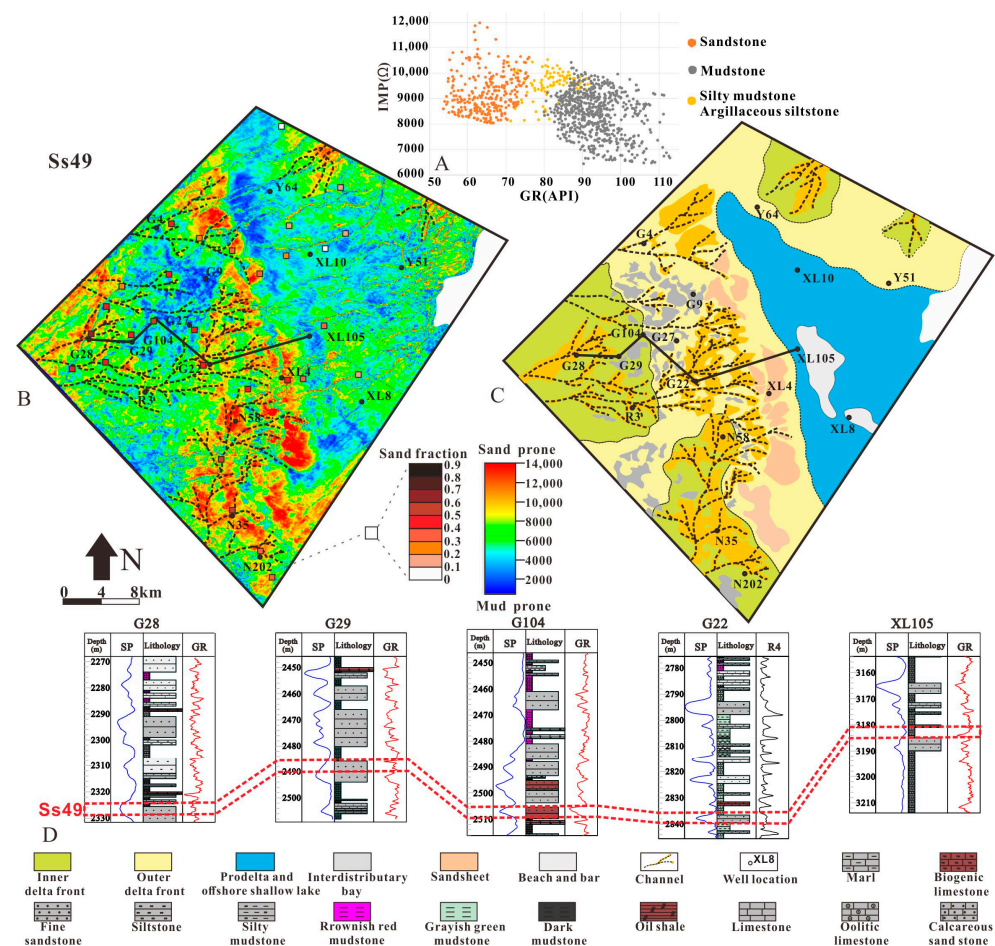


Figure 6. RMS amplitude stratal slices (Ss49) and corresponding interpretations. (A) Relationship between lithology and impedance. (B) RMS amplitude stratal slice (Ss49) extracted in upper fourth member of Shahejie Formation; box in (A) represents ratio of sand to strata. (C) Interpretation of (B). (D) Well profile used to calibrate lithologies in (B).

The RMS amplitude stratal slice Ss05 (Figure 7A), extracted from Mbr 4^L of the Shahejie Fm, is interpreted as exhibiting three shallow-water deltas with generally lobate planforms and a network of subaqueous distributary channel fills in the preserved inner delta front. The distributary channel fills have an average sinuosity of ca. 1.1 and exhibit evidence of possible lateral accretion and meandering planforms, and the width of the channel belt is in the range of 318–1375 m. This region extends about 15–25 km basinward, whereas the deltas cover an area of 1168 km². The southern part of the study area, especially the southwestern region, is covered by a large domain with a high RMS amplitude character, indicating a prevalence of sand-prone lithologies. These units are connected and extend into the basin towards the northeast direction and are interpreted as the deposits of subaqueous distributary channels in the inner delta front (Figure 7B). The well log profiles of wells G28, G29, G104, and XL105 demonstrate that these wells intersect sand-rich units on Ss05 and support the interpretation of a subaqueous distributary channel origin. In contrast, well G22 indicates the presence of mud-prone units, with well log signatures that make them interpretable as distributary-bay deposits (Figure 7C). In the central area of the RMS attribute slice, intermediate RMS amplitude characters dominate, but a sporadic occurrence of small-scale units with high RMS amplitude is seen; this area is interpreted as the deposits of the outer delta front, characterized by heterolithic deposits with a limited sand content. This interpretation is also supported by well log and core observations. The northern area characterized by low RMS amplitude values is dominated by units with a high mudstone content, which are interpreted as having accumulated in offshore shallow-lake settings.

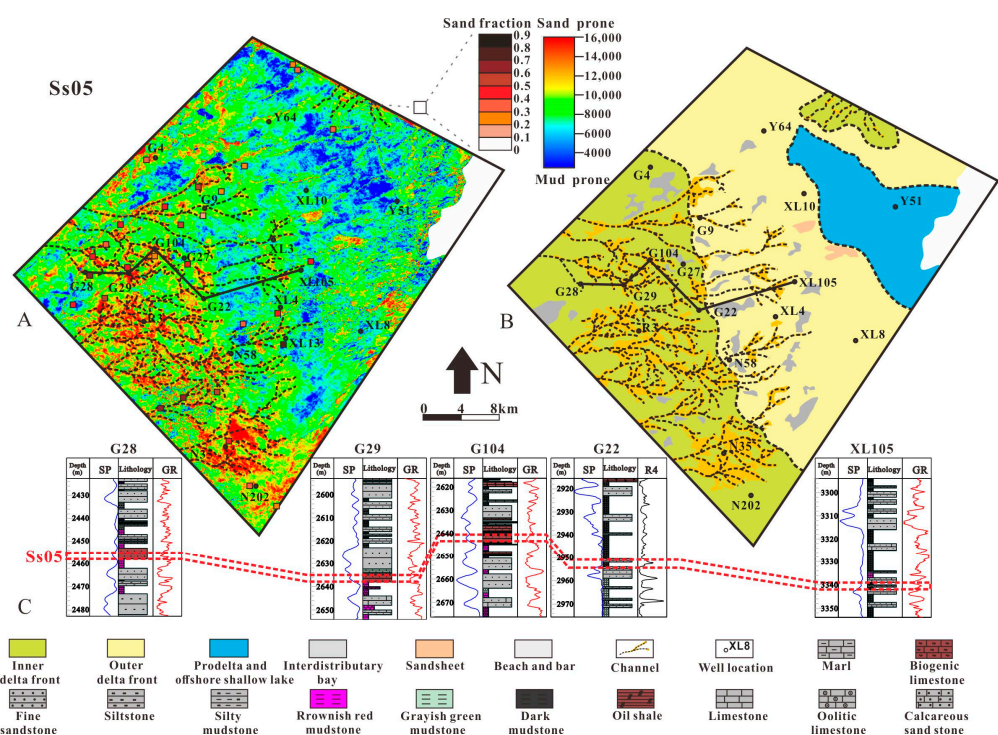


Figure 7. RMS amplitude stratal slices (Ss05) and corresponding sedimentary interpretations. (A) RMS amplitude stratal slice (Ss05) extracted in lower fourth member of Shahejie Formation; box in (A) represents ratio of sand to strata. (B) Interpretation of (A). (C) Well profile used to calibrate lithologies in (B).

4.3. Controlling Factors Affecting the Shallow-Water Deltas

The lacustrine shallow-water deltaic systems developed in the Mbr 4 of the Shahejie Fm on the hanging-wall ramp of the Raoyang Sag were likely controlled by the interplay of different factors. Here, we consider data that help elucidate the influences exerted

by paleotopography, climate changes, and resulting variations in water discharge and sediment supply.

4.3.1. Basin Paleotopography

The reconstruction of paleotopographic characteristics of the basin and associated source areas is essential for relating stratigraphic architectures to the evolution of sediment sources and sediment routing systems [69–73].

In this study, the paleotopography of the basin in the study area was characterized using 3D seismic data. Since very limited erosion restricted to the northeastern part of the study area occurred during the deposition of Mbr 4 of the Shahejie Fm, no restoration of formation denudation was performed in this study. For the interval with T₃ as the top and T₄ as the base, a thickness map was obtained as a general indicator of the paleotopographic features of Mbr 4 of the Shahejie Fm based on time–depth conversion and sediment decompaction according to porosity–depth curves (Figure 8A). The resulting map shows that the interval thickens gradually to the east in relation to a regular slope profile. High-relief terrain existed in the western sector. Based on stratigraphic correlation, 10 wells and five profiles along the paleoslope were selected (Figure 8B). By flattening the top surface, T₃ (Figure 8C), and operating a decompaction considering the different lithologies of the target interval, the original thickness of the target layer was calculated; measuring the horizontal separation between two wells, the gradient of the surface could then be calculated (Figure 8D). The results show that the average gradient of the slope of the hanging-wall dip slope is 0.015 m/m. This is consistent with the slopes of many deltaic systems recognized globally, such as the deltaic units of the Dongying Formation in the Baxian Sag of the Bohai Bay Basin, which exhibits a slope gradient of *ca* 0.95° [74], or the Cretaceous shallow-water deltaic system of the Songliao Basin, with a slope < 1°. This form of gentle topography provides favorable topographic conditions for the deposition of shallow-water deltas.

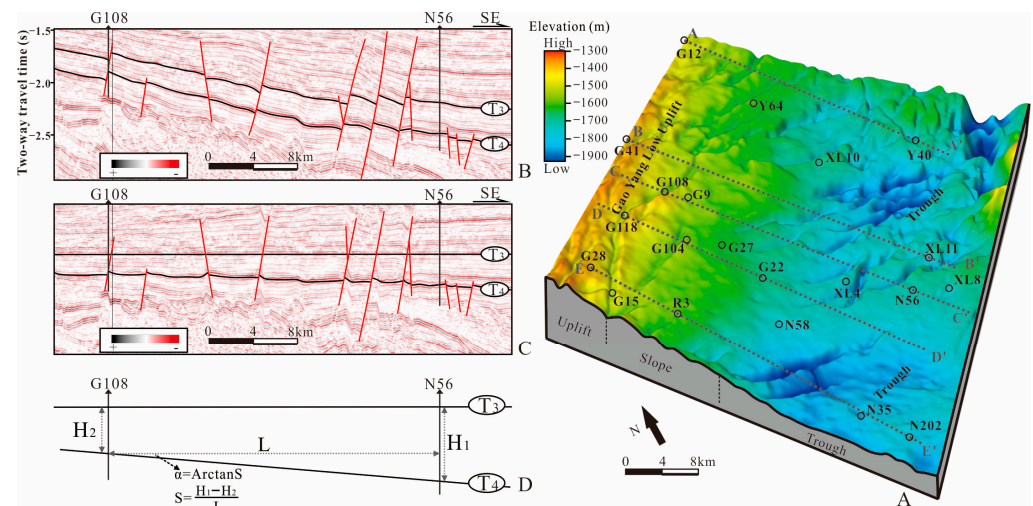


Figure 8. Paleotopographic features of the fourth member of the Shahejie Formation before deposition on the hanging-wall ramp of the Raoyang Sag. (A) A paleotopographic map. The red dotted curves indicate the boundaries of different tectonic units. The gray dotted lines indicate the five seismic profiles used to measure the original gradients. (B) The original seismic profile used to measure gradients. The location of the profile is shown in (A), marked in gray dotted lines, C–C'. (C) The seismic profile was flattened to T₃. (D) A diagram illustrating the approach to gradient measurement. H₁ and H₂ indicate the decompacted stratal thickness of N56 and G108, respectively; L is the distance between the two wells, α is the slope angle, and S is the gradient. A–A', B–B', C–C', D–D', E–E' are profiles used to measure slopes.

4.3.2. Paleohydrology and Water Conditions

The intensity of sunlight entering the water, by affecting photosynthesis, controls the survival of microalgae, which are extremely sensitive to changes in water depth [75]. This study used the weighted average of contents of algae fossils to estimate the water depth of the paleolake [76]:

$$h_{\min} = (4x + 4y) / (x + y + z) \quad (1)$$

$$h_{\max} = (10x + 10y + 2z) / (x + y + z) \quad (2)$$

where x , y , and z are the contents of *Granulosus*, *Reticulosus*, and *Leiosphaeridia*, respectively.

The analysis of palynological data of 83 mudstone samples (11% from the flood plain deposits, 66% from the front interdistributary bay deposits, and 23% from the prodelta and lacustrine mudstone) shows that the algae content is limited in Mbr 4^L of the Shahejie Fm, for which the average water depth of the lake was estimated to be between 2.00 m and 8.22 m. Vertical or subvertical burrows are seen, which are usually due to the behavior of organisms responding to energetic hydrodynamic conditions in shallow-water areas [76,77]. Algae become abundant in the interval of Mbr 4^M of the Shahejie Fm, for which the water column is interpreted to have deepened, with an average water depth ranging between 2.72 and 10.00 m. In addition, thick dark mudstone succession can be observed in the eastern coreholes, which supports the idea of deeper bathymetry. Algae are also abundant in the interval of Mbr 4^U of the Shahejie Fm, which was deposited at times when the water was relatively shallow, with an average water depth varying between 1.40 and 9.95 m. The lithological characteristics of the Mbr 4^U of the Shahejie Fm are characterized by upper mudstones that are mostly brownish red, and middle and lower mudstones that are commonly brownish red, gray, or grayish-green. The diversity of fossil taxa (genera and species) has a particular relationship with the water depth at the time of deposition, which can be used to infer the sedimentary environment [33,78]. In this study, we also used the diversity of ostracods to calculate the paleo-water depth [33]. A commonly used index termed information function entropy, $H(s)$, is defined as follows [33,50,79]:

$$H(s) = - \sum P_i \ln P_i \quad (3)$$

where P_i is the proportion given by the number (n_i) of the ' i ' species in the total number ' N ' of the whole group of ostracods.

$$P_i = n_i / N \quad (4)$$

The analysis of ostracod data of 64 mudstone samples (3% from the flood plain deposits, 67% from the front interdistributary bay deposits, and 31% from the prodelta and lacustrine mudstone) shows that the average $H(s)$ values for ostracods in intervals of Mbr 4^L, Mbr 4^M, and Mbr 4^U of the Shahejie Fm are 0.52, 0.76, and 0.47, respectively. Based on a relationship between the water depth and $H(s)$ proposed by [33], and considering the mudstone color, it is concluded that the average water depths of the lake during the times of deposition of Mbr 4^L, Mbr 4^M, and Mbr 4^U of the Shahejie Fm were 4.3 m, 8.2 m, and 4.1 m, respectively; this quantification portrays a deepening then shallowing trend (Figure 9).

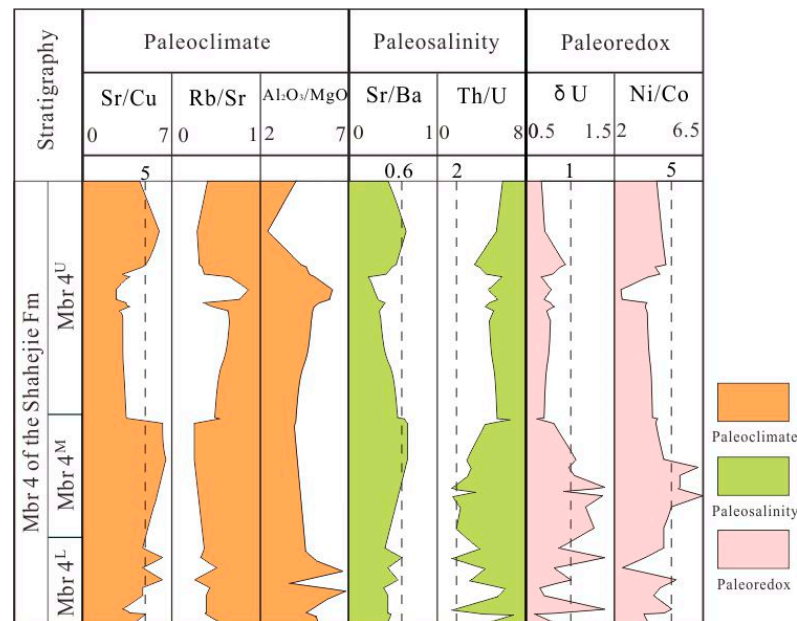


Figure 9. Stratigraphic variations in major elements and trace elements in mudstones of fourth member of Shahejie Formation as indicators of environmental change. Data on 56 mudstone samples.

Paleosalinity and Redox Conditions

In both modern and ancient lakes, Sr/Ba is positively correlated with salinity due to the stronger migration of Sr in the solution compared to Ba [80–83]. It should be noted that the amount of carbonate content in mudstone has a great influence on the Sr content, and mudstone samples with a high carbonate content are more likely to enrich Sr [83]. In addition, Th is easily adsorbed by clay minerals, and U easily leaches or oxidizes, so the Th/U ratio in marine sediments is less than 2, while the Th/U ratio in terrestrial sedimentary environments is larger. In this study, Sr/Ba and Th/U were used to determine the paleosalinity of the lake. The analysis of trace element data of 56 mudstone samples (4% from the flood plain deposits, 70% from the front interdistributary bay deposits, and 27% from the prodelta and lacustrine mudstone) shows that, in the Mbr 4^L period, the study area was characterized by a brackish water environment. The salinity of the lake increased during the deposition of Mbr 4^M and then decreased during the deposition of Mbr 4^U when a freshwater environment was predominant (Figure 9).

The Ni/Co and δU values are reliable indicators of oxidative reduction in sedimentary environments [53–55]. The solubility of Ni and Co is controlled by the redox state in the environment. Among them, Co readily dissolves under oxidizing conditions and becomes enriched under reducing conditions. A Ni/Co ratio greater than 7 usually indicates a very anoxic environment, whereas values between 5 and 7 indicate a slightly reducing environment, and values lower than 5 indicate an oxygen-rich environment [53]. In addition, Th and U are sensitive to both the salinity of the sedimentary environment and its redox state [53,84]; Th is not affected by the redox conditions of the sedimentary environment and remains insoluble as Th⁴⁺; U exists as insoluble U⁴⁺ under highly reduction conditions and soluble U⁶⁺ under oxidizing conditions, resulting in the loss of U in sediments. In a normal water environment, δU is less than 1, and in an anoxic environment, δU is greater than 1 [53,84].

$$\delta U = U / [0.5 * (Th/3 + U)] \quad (5)$$

In combination with observations on the mudstone color, the data indicate that Mbr 4^L of the Shahejie Fm interval in the study area was deposited in a setting dominated by

oxidizing conditions, that Mbr 4^M accumulated in a slightly reducing environment, and that Mbr 4^U accumulated in an oxidizing environment (Figure 9).

4.3.3. Paleoclimate

During the Himalayan orogenic period, when the Shahejie Fm was deposited, the Bohai Bay Basin experienced multiple episodes of lake expansion and contraction [32,33], acting in accordance with paleoclimatic changes. The development of vegetation is directly controlled by climate and its geographic variations and is particularly sensitive to temperature and humidity. Pollen is light and readily preserved in sediments in which assemblages and the abundance of sporopollen can be employed as indicators of paleoclimate [15,85,86]. By analyzing the characteristics of the sporopollen assemblages as temperature indicators together with the geochemical composition of the sediments, the paleoclimate during the deposition of Mbr 4 of the Shahejie Fm in the study area was studied.

A total of 150 sporopollen species were found in 83 samples from nine wells in the Shahejie Fm in the study area. These mainly consist of angiosperms (43.43–61.88%), of which *Quercoidites* (11.1–21.79%) and *Ulmipollenites* (10.48–11.37%) are dominant. Gymnosperms (22.60–28.87%) are abundant, whereas ferns (4.73–16.05%) and algae (3.68–17.88%) are subordinate (Figure 10A). The sporopollen assemblages have vertical zonation. Specifically, when Mbr 4^L of the Shahejie Fm was deposited, mesophytes were the dominant species (68.35%), among which *Quercoidites* and *Ulmipollenites* dominated. There were relatively few hygrophytes, phreatophytes, and helophytes (18.48%). Palynolites (7.47%) typical of arid climates, such as *Ephedra* and *Chenopodipollenites*, also appeared (Figure 10B) [15,87,88]. Subtropical plants (32.84%) and temperate plants (25.37%) were abundant (Figure 10C), and this may be a characteristic inherited by climatic conditions that predated the deposition of Mbr 4 of the Shahejie Fm.

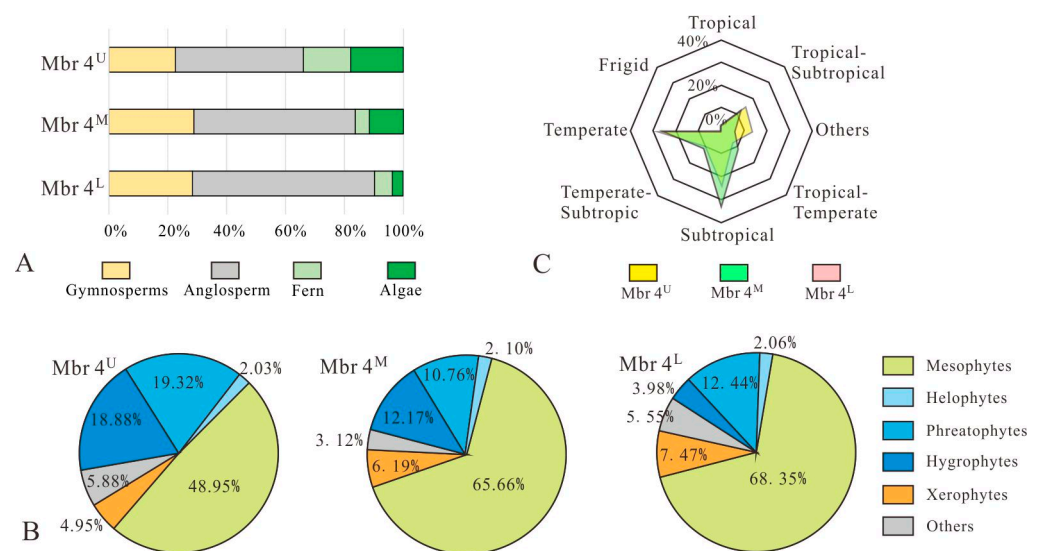


Figure 10. Sporopollen characterization of fourth member of Shahejie Formation. (A) proportions of different types of vegetation; (B) Pie charts of vegetation proportions in different ecological environments. (C) I Radar map of vegetation proportions across different climatic zones.

When Mbr 4^U of the Shahejie Fm was deposited, mesophytes were still dominant (65.66%). However, hygrophytes, phreatophytes, and helophytes increased significantly in proportion (25.02%) compared with the earlier times of Mbr 4^L; the relative content of algae also increased (11.64%), whereas xerophytes such as *Ephedra* decreased (6.19%) (Figure 10B). Temperate (24.73%) and subtropical (33.86%) vegetation predominated (Figure 10C). These characteristics indicate a relatively humid, transitional climate.

In Mbr 4^U of the Shahejie Fm, the numbers of hygrophytes, phreatophytes, and helophytes increased significantly (40.23%), mainly in the genera *Sphaerotilus* and *Salicornia*; mesophytes were most represented (48.95%), while xerophytes were subordinate (4.95%) (Figure 10B). Temperate (27.93%) and subtropical plants (23.69%) were still dominant (Figure 10C).

In summary, the palynological data testify to a progressive increase in humidity from the Mbr 4^L to Mbr 4^U phase, when the climate gradually shifted from subtropical to temperate and subtropical.

The concentrations of major and trace elements in mudstone sediments tend to vary as a function of the paleoclimate, and their ratios are important indicators of paleoclimate change [43,44,46,82,89]. Sr is enriched in arid conditions, while Cu is enriched in humid conditions; the Sr/Cu ratio in a warm and humid climate is in the range of 1.3 to 5, and a Sr/Cu ratio greater than 5 indicates a hot and dry climate [43,47]. In chemical weathering, Rb is relatively stable, while Sr is easily weathered, so the Rb/Sr value is high in a humid environment and low in an arid environment [45,46]. The Al₂O₃/MgO ratio can also reflect climatic changes during deposition. Larger values of this ratio indicate a warmer and more humid climate, whereas smaller values indicate a drier climate. The Sr/Cu, Rb/Sr, and Al₂O₃/MgO values obtained by calculation by major elements and trace element data of 56 mudstone samples (4% from the flood plain deposits, 70% from the front interdistributary bay deposits, and 27% from the prodelta and lacustrine mudstone) are shown in Figure 9. A comprehensive analysis of these geochemical data can be interpreted as a record of a climate that was gradually becoming more humid from the early to the late stage of Mbr 4. The quantitative analysis of the paleoclimate based on the Sr/Cu, Rb/Sr, and Al₂O₃/MgO ratios reflects climate differences in terms of relative, rather than absolute, climate conditions; this analysis is therefore complemented by a palynological analysis.

4.3.4. Sediment Supply

The hydraulic characteristics of the formative rivers of fluvial successions can tentatively be inferred on the basis of sedimentological observations that can be made on sediment cores [58,59]; this approach is also applicable to the fluvial deposits of deltaic successions [90,91]. Thickness measurements of individual sets of mesoform cross-bedding made in the core have been applied to empirical relationships [57–60] for estimating paleohydrological and geomorphic parameters of deltaic distributary channels, such as the channel depth, channel width, channel belt width, and bankfull discharge (Table 2).

Table 2. The ranges and mean values (‘avg’) of the measured and inferred characteristics of the distributary channels of the studied lacustrine shallow-water deltas of the fourth member of the Shahejie Formation, Raoyang Sag, Bohai Bay Basin.

Predicted Variable	Mbr 4 ^U	Mbr 4 ^L
Cross-set thickness (Sm/cm)	7.1–20.1, avg 12.5	8.8–21, avg 13.7
Dune height (Bm/m)	0.21–0.59, avg 0.37	0.26–0.62, avg 0.4
Channel mean bankfull depth (Dm/m)	1.19–3.37, avg 2.09	1.47–3.52, avg 2.3
Channel width (Wc/m)	12.28–81.05, avg 35.89	18.06–87.93, avg 42.06
Channel belt width (Wcb/m)	82.54–533.58, avg 238.12	120.86–578.39, avg 278.6
Channel width-to-depth ratio	10.28–24.05, avg 16.16	12.23–24.95, avg 17.49
Bankfull discharge (Q _{bf} /m ³ s ^{−1})	77.14–2825.13, avg 736.29	155.09–3184.96, avg 913.66

Bankfull discharge (Q_{bf}) is defined by

$$Q_{bf} = UA \quad (6)$$

where Q_{bf} is the bankfull water discharge ($\text{m}^3 \text{s}^{-1}$), A is the channel bankfull cross-sectional area (m^2), and U is the mean flow velocity at bankfull conditions (m s^{-1}), as estimated using the Chezy equation [59].

$$U = C_Z * (RS)^{\frac{1}{2}} \quad (7)$$

where C_Z is the Chezy Coefficient, R is the hydraulic radius (m), and S is the stream gradient. C_Z is defined as

$$C_Z = g^{\frac{1}{2}} * 8.1 * (D_m / K_s)^{\frac{1}{6}} \quad (8)$$

where D_m is the mean bankfull water depth (m), and K_s is the roughness element:

$$K_s = 3D_{90} + 1.1B_m(1 - \exp^{-25\psi}) \quad (9)$$

where D_{90} is the 90th centile of grainsize distribution, whereas B_m is the bedform (e.g., alluvial dunes, and transverse bars) height (m) [58,59,90], and ψ is the ratio of the bedform height and bedform wavelength (Van Rijn, 1984).

$$B_m = 5.3\beta + 0.001\beta^2 \quad (10)$$

$$\beta \approx S_m / 1.8 \quad (11)$$

$$\psi = B_m / \lambda \quad (12)$$

where S_m is the cross-set thickness (m), β is the thickness of the unpreserved (eroded) upper portion of the bedform (m), and λ is the bedform wavelength (m) (Van Rijn, 1984), for which

$$\lambda = 7.3D_m \quad (13)$$

where D_m is the channel's mean bankfull depth (m), and D_{max} is the maximum (thalweg) channel bankfull depth (m) [56,57].

$$D_m = 0.57D_{max} \quad (14)$$

$$D_{max} \approx 10B_m \quad (15)$$

$$R = A / L \quad (16)$$

where L is the channel perimeter. For ease of calculation, this study assumes channel profiles are semi-elliptical in shape, for which the following applies:

$$A = \frac{1}{2}\pi * D_m * W_c \quad (17)$$

$$L = \pi W_c + 2(D_m + W_c) \quad (18)$$

where W_c is the channel width (m). The relationship between W_c and the channel depth (D_m) is [58]

$$W_c = 8.88(D_m)^{1.82} \quad (19)$$

By analyzing the cross-bedded sets from 201 sandstone samples from 62 channel fills (22% from subaerial distributary channel fills and 82% from subaqueous distributary channel fills), it is observed that the cross-bedded sets show thicknesses ranging between 8.8 and 21.0 cm, with an average of 13.7 cm. The estimated bankfull discharge ranges between 155 and 3185 $\text{m}^3 \text{s}^{-1}$, with an average of 914 $\text{m}^3 \text{s}^{-1}$. In interval Mbr 4^U of the Shahejie Fm, the thickness of the cross-bedded sets is between 7.1 and 20.1 cm, with an average of 12.5 cm; the estimated bankfull discharge is between 77 and 2825 $\text{m}^3 \text{s}^{-1}$, with an average of 736 $\text{m}^3 \text{s}^{-1}$. It must nonetheless be considered that there is significant uncertainty

in estimating discharge empirically using core data [60]. This approach is influenced by several significant limitations, especially in relation to the complexity of the preservation of bedforms as cross-strata, to the variability of controls on the mesoform type and size, and to the variability in the scaling of bedforms, water depth, and river discharge.

As a complementary analysis, the sandstone fraction and average accumulation rates are examined using data from 63 wells.

5. Discussion

5.1. Factors Governing the Studied Shallow-Water Deltas

Various factors, including the climate and basin tectonics, may control relative lake-level fluctuations. In turn, changes in lake level control the architecture and stratigraphic distribution of deltaic sandbodies [18,22,92].

The results indicate that the paleotopography on which the studied deltas formed was characterized by relatively gentle relief during the time of deposition of Mbr 4^L of the Shahejie Fm, and that the rift basin was undergoing expansion during the early phase of Mbr 4^L deposition. The results also suggest that the rate of sediment supply might have been relatively high, that the climate was humid, and that the lake was relatively shallow. At this stage, extensive delta front deposition took place, before a time when the lake level rose rapidly, resulting in delta retrogradation [27]. During Mbr 4^U, the basin was in a post-rift stage, the rate of sediment supply decreased, the climate became more humid, and the lake level was higher but underwent a slow fall through time. At this time, delta front deposits with limited extent were accumulated as the delta prograded into the basin.

According to the attempted quantifications, the rate of sediment supply was more sustained during the Mbr 4^L phase compared to the Mbr 4^U phase. This may seem inconsistent with an inference of a more humid climate for Mbr 4^L of the Shahejie Fm, but it may be related to a temporal variation in tectonic activity [20]. The shift from active rifting during the Mbr 4^L phase to a post-rift phase during Mbr 4^U may have affected the physiography of the deltaic catchments, which might have been characterized by relatively higher relief during the Mbr 4^L phase. The humid climate might have favored the chemical weathering in the catchments, resulting in a substantial sediment supply [93]. As an essential structural element of the Jizhong Depression, the Taihang Mountains Piedmont fault controlled the formation of the Jizhong Depression and the uplift of the Taihang Mountains [94]. Previous studies on the piedmont faults of Taihang Mountain demonstrated that during the deposition of members Mbr 2 and Mbr 3 of the Shahejie Fm, predating the Mbr 4 phase, fault activity was higher, and faults were larger; additionally, fault activity significantly weakened, and faults became smaller during the deposition of Mbr 4 and the Doingying Fm [94]. Therefore, exposed bedrock source areas in the Taihang Mountains may have been smaller during the deposition of Mbr 4^U of the Shahejie Fm, resulting in a relatively reduced sediment supply.

5.2. Evolution of Distributary Channel Networks and Implications for Sandbody Architectures

Two types of distributary channel systems have been documented in Mbr 4 of the Shahejie Fm interval of the Raoyang Sag. During the Mbr 4^L period, the rift basin was expanding, the climate was humid, the rate of sediment supply was relatively high, the extent of the lake was limited, the lake level was low, and the rate of relative lake-level rise was rapid; these conditions favored the formation of shallow-water deltas undergoing steady retrogradation (Figure 11A). The relatively high sediment supply enhanced the lateral mobility of the channels as well as their frequent avulsion. In addition, the progradation rate and the size of the drainage network may also affect the split frequency of the channels [95]. Avulsive splits and bifurcations of the channels resulted in a large

number of distributaries occupying the delta plain, which are now preserved as a network of composite amalgamated sandbodies. The deltas extended into the lake basin for a distance of up to 15 to 25 km and were characterized by large delta front areas. The sinuous planform of some of the channel bodies may reflect the progressive growth of meander bends [96,97], whereas the vertical stacking of multiple channel forms with erosional bases is reflected in the observation of multiple fining-upward trends. This phenomenon may indicate the re-occupational avulsion of asynchronous channels [95]. This process is documented in many modern deltas [98–100]. Individual channel fills are dominantly made of fine sandstone. Sandstone connectivity is therefore facilitated by the amalgamation of different channel bodies, which may be caused by confluences that existed between coeval channels and the cannibalization of channel deposits by younger channels. Towards the basin, the superposition of sandbodies changes from lateral mutual cutting to isolation.

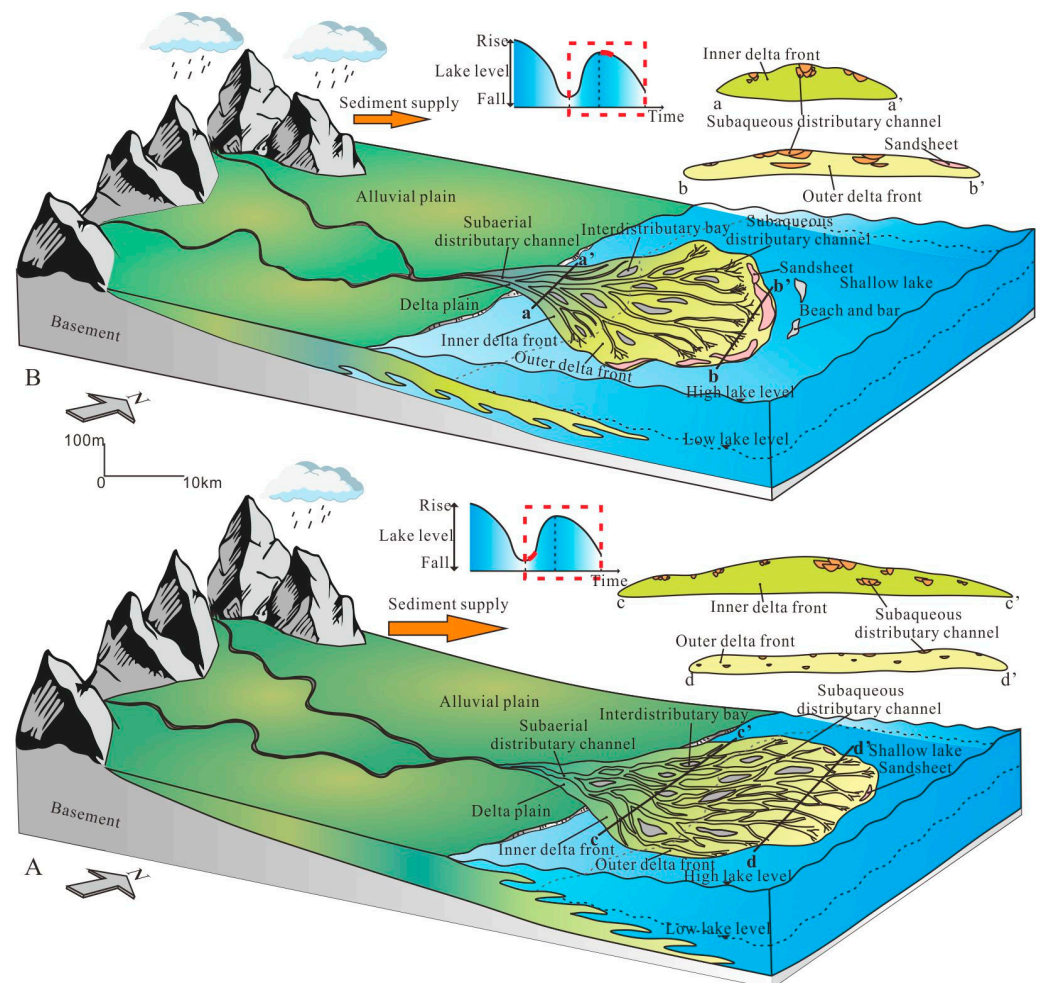


Figure 11. Depositional models of the lacustrine shallow-water deltas of the lower (A) and upper areas of the fourth member of the Shahejie Formation (B). a-a', b-b', c-c' and d-d' are profiles through different parts of the delta.

During Mbr 4^U, the basin entered a post-rift phase. The lake water was dominated by freshwater, the climate was relatively humid, and terrestrial areas were densely vegetated; the lake covered an extensive area, and the lake level was high and gradually falling at a slow rate. The shallow-water deltas extended for up to 17 to 22 km into the basin (Figure 11B). Compared with the Mbr 4^L phase, the rate of lateral channel migration was lower, meaning that channels were relatively stable; the distributaries mainly underwent vertical aggradation and bifurcation, forming a ramiform network of low-sinuosity chan-

nels. At channel mouths, flow expansion into the lake facilitated the formation of a large number of bifurcations and the deposition of sediment that was readily reworked by waves into continuous shore-parallel sandsheets in the outer delta front [9]. The channel bodies mainly present a vertical stacking pattern, with individual channel fills exhibiting a limited sandstone content. Physically connected channel bodies exhibit both sandstone–sandstone and sandstone–mudstone contacts in relation to the presence of in-channel mudstone deposited under low-energy conditions in distributary channels [13]. Towards the basin center, the sandbodies become increasingly more isolated.

5.3. Applied Subsurface Resource Potential

The presence of sealing faults, the local preservation of paleorelief, and the architecture of sedimentary systems all influence the types and distributions of traps for fluids in the subsurface [22,101,102]. On the hanging-wall ramp of the Raoyang Sag, the terrain is higher in the west than in the east. As the west is close to the boundary of the sag, faults are well developed in that area; the number of faults decreases towards the east [37]. Consequently, the hanging-wall ramp of the Raoyang Sag is conducive to the development of structural traps, structural-lithologic traps, and lithologic traps [37,101,102].

Two types of shallow-water deltas are recognized to have developed during the Shahejie Fm phase on the hanging-wall ramp of the Raoyang Sag, which are characterized by morphological differences in their distributary channels. In Mbr 4^U, a dendritic network of channel bodies is characteristic of the shallow-water delta in which sandstone bodies are especially preserved in the outer delta front region. The sand fraction of this succession ranges from 0.07 to 0.64 (Figure 6B; Table 3). The vertical juxtaposition of subaqueous distributary channels, sandsheet, and prodelta and lacustrine mudstones favors the formation of structural–lithologic traps and lithologic traps [101,102], which mainly consist of sandstone up-dip pinch-out traps and sandstone lens traps (Figure 12).

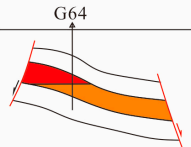
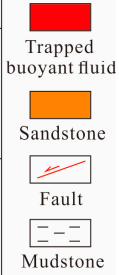
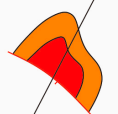
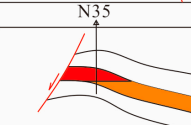
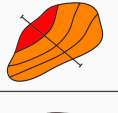
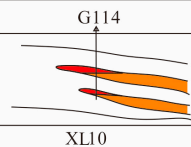
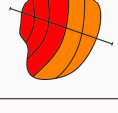
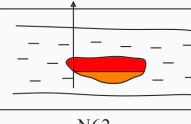
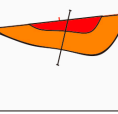
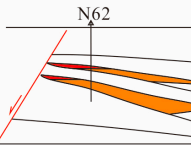
Trap type		Plan	Section	
Structural Trap	Fault-block Trap			
	Fault-nose Trap			
Lithologic Trap	Sandstone Up-Dip Pinch-out Trap			
	Sandstone Lens Trap			
Composite Trap	Structural-Lithologic Trap			

Figure 12. Fluid trap types in the fourth member of the Shahejie Formation, Raoyang Sag, Bohai Bay Basin.

Table 3. Characteristics and trapping style of reservoir-quality sandstone of studied lacustrine shallow-water deltas of fourth member of the Shahejie Formation, Raoyang Sag, Bohai Bay Basin.

Stratum	Mbr 4 ^U	Mbr 4 ^L
Type of deltas	Shallow-water deltas with dendritic distributary channel networks	Shallow-water deltas with reticular distributary channels
Sandstone-rich facies belt	Outer delta front	Inner delta front
Typical reservoir-quality facies association	Subaqueous distributary channel, sandsheet	Subaqueous distributary channel
Sand fraction	0.07–0.64, avg 0.37	0.15–0.84, avg 0.45
Net-to-gross ratio	0–0.29, avg 0.06	0–0.46, avg 0.13
Contact relationship of sandbodies	Sandstone is in vertical contact with prodelta and lacustrine mudstones	Subaqueous distributary channel sandbodies crosscut each other
Trap	Structural–lithologic trap, sandstone up-dip pinch-out trap, sandstone lens trap	Fault-block trap, fault-nose trap, structural–lithologic trap, sandstone up-dip pinch-out trap

In the stratigraphy of Mbr 4^L, reservoir-quality sandbodies are mainly associated with a reticular channel body network of the shallow-water delta in which sandstone is concentrated in the inner delta front. The sand fraction (ranging from 0.15 to 0.84) of this type of shallow-water delta succession is higher than that of dendritic shallow-water deltas (Figure 7B; Table 3). In the western part, affected by faults, structural traps are formed, mainly including fault-block traps and fault-nose traps. In the eastern part, where there are fewer faults, lithologic traps are mainly developed, along with a small number of structural–lithologic traps. Due to the processes of the lateral migration, avulsion, and bifurcation of distributary channels, the connectivity of sandbodies in this part of the strata is higher than in other intervals. As a result of the amalgamation of the deposits of distributary channels, the composite sandbodies in the inner delta front region of shallow-water deltas are laterally continuous, forming potentially attractive subsurface reservoir volumes. In combination with the laterally extensive mudstones of Mbr 4^M, sandstone up-dip pinch-out traps are formed [101,102] (Figure 12). Therefore, the successions of shallow-water deltas with a reticular distributary channel network may have higher fluid-trapping potential than shallow-water deltas with a dendritic distributary channel network.

In view of the discussion above, it is apparent that shallow-water deltaic successions of the Raoyang Sag have potential as possible repositories for carbon capture and storage (CCS). The shallow-water deltas of the Raoyang Sag formed on the hanging-wall ramp of a rift basin, where sediment carried by rivers was transported downslope and accumulated under the action of lacustrine processes. The studied delta front deposits are characterized by significant lateral extent, a high sandstone content, good sorting, medium to high porosity (7.5–25.1%) [101], and the presence of secondary pores due to intergranular and intragranular dissolution; these aspects make the studied succession a potential reservoir for CO₂ storage. At the same time, the lacustrine mudstone of Mbr 4^M is characterized by large thickness (50–150 m), good continuity, and good sealing capacity, which can effectively prevent the upward migration of CO₂. In addition, the mixed-layer clay mineral content of illite and montmorillonite in this mudstone is 40% on average [103]; this may enhance adsorption capacity and determine low permeability, thus strengthening the sealing effect on injected CO₂ migration. In summary, this study supports the idea that the Mbr 4 shallow-water deltaic lacustrine succession can be used as a potential large-scale CO₂ storage reservoir in the Bohai Bay. Further evaluations of reservoir and cap structure are needed in the future to better assess and minimize the risk of CO₂ leakage in any such program.

6. Conclusions

Mbr 4 of the Shahejie Fm in the Raoyang Sag was deposited on a hanging-wall ramp, characterized by a paleotopography dipping from west to east. During Mbr 4, the climate changed from a relatively arid subtropical climate to a relatively humid temperate and subtropical climate. The sediment feeding the deltas was mainly delivered from the southwest. The rate of sediment supply was continuous in the early stage and gradually weakened in the later stage of Mbr 4 accumulation. The water of the lake near the shore platform was shallow with an average depth of less than 10 m, and the lake level showed a trend of rapid rise followed by slow fall. Mbr 4^M of the Shahejie Fm was dominated by open-lake deposits, whereas Mbr 4^U and Mbr 4^L of the Shahejie Fm were mainly composed of lacustrine shallow-delta deposits.

Two types of shallow-water deltaic successions have been recognized in Mbr 4 of the Shahejie Fm in the study area. When the basin was in the active rift stage, the sediment supply was relatively high, resulting in a broader shallow-water delta front. The distributary channels were likely mobile and sinuous. The distributary channels formed an intricate reticular distributary network, associated with an inner delta front region with a higher sandstone fraction, forming sandstone up-dip pinch-out traps. When the basin entered the post-rift stage, the sediment supply rate decreased. At this time, the shallow-water delta front was less extensive, showing a dendritic distributary channel network. The distributary channels were relatively stable, with reduced lateral migration and decreased sinuosity. In the outer delta front region, the sediment was readily reworked into sandsheet. The vertical stacking of these sandbodies with prodelta and lacustrine mudstones has led to the formation of sandstone up-dip pinch-out traps and sandstone lens traps. This study reveals the influence of multiple factors on the sedimentary characteristics, evolution, and internal anatomy of shallow-water deltas that developed at different stages of rift-basin evolution and highlights their resource potential in terms of subsurface reservoir characteristics. In the context of a sustainable energy transition, the results of this study provide a basis for planning the implementation of CCS programs in deltaic successions of the Bohai Bay.

Author Contributions: Writing—original draft preparation, L.Y.; writing—review and editing, N.P.M. and L.C.; visualization, S.X. and R.Z.; supervision, X.Z. All authors have read and agreed to the published version of the manuscript.

Funding: This research was funded by the National Natural Science Foundation of China: Study on the Configuration and Formation Mechanism of Estuarine bar in the front of Lacustrine Fan Delta, 42272110 (2023–2026).

Institutional Review Board Statement: Not applicable.

Informed Consent Statement: Not applicable.

Data Availability Statement: The original contributions presented in this study are included in the article; further inquiries can be directed to the corresponding author.

Acknowledgments: The authors thank the anonymous reviewers for providing critical comments and suggestions that improved the manuscript and thank the Huabei Oilfield Branch Company of PetroChina for their support.

Conflicts of Interest: Author Renhao Zhang was employed by the company China JIKAN Research Institute of Engineering Investigations and Design, Co., Ltd. The remaining authors declare that the research was conducted in the absence of any commercial or financial relationships that could be construed as a potential conflict of interest.

References

1. Mann, P.; Gahagan, L.; Gordon, M. Tectonic setting of the world's giant oil and gas fields: Giant oil and gas fields of the decade 1990–1999. *AAPG* **2003**, *78*, 15–105.
2. Selim, S.S. Sedimentological model, architecture, and evolution of a shallow-water Gilbert-type delta from the Lower Miocene, Red Sea Rift, Egypt. *Int. Geol. Rev.* **2020**, *62*, 2053–2076. [[CrossRef](#)]
3. Sohn, Y.K.; Kim, S.B.; Hwang, I.G.; Bank, J.J.; Choe, M.Y.; Chough, S.K. Characteristics and depositional processes of large-scale gravelly Gilbert-type foresets in the Miocene Doumsan fan delta, Pohang Basin, SE Korea. *J. Sediment. Res.* **1997**, *67*, 130–141.
4. Azennoud, K.; Baali, A.; Joanes, M.F.; Asmi, E.H.; Brahim, A.Y. Disentangling orbital, sub-orbital, and tectonic signatures from lacustrine sediments developed upon a half-graben (Lake Ifrah Basin, Northwest Africa): Insights into lowest-rank T-R sequences in accommodation basins. *Sediment. Geol.* **2023**, *449*, 106376. [[CrossRef](#)]
5. Gawthorpe, R.L.; Colella, A.; Prior, D.B. Tectonic Controls on Coarse-Grained Delta Depositional Systems in Rift Basins. In *Coarse-Grained Deltas*; Colella, A., Prior, D.B., Eds.; IAS Wiley: Oxford, UK, 1990; pp. 113–127.
6. Muravchik, M.; Bilmes, A.; D'elia, L.; Franzese, J.R. Alluvial fan deposition along a rift depocenter border from the Neuquen Basin, Argentina. *Sediment. Geol.* **2014**, *301*, 70–89. [[CrossRef](#)]
7. Bhattacharya, J.P.; Willis, B.J. Lowstand deltas in the Frontier Formation, Powder River Basin, Wyoming: Implications for sequence stratigraphic models. *AAPG Bull.* **2001**, *85*, 261–294.
8. Martini, I.; Sandrelli, F.; Ambrosetti, E. Shoal-water deltas in high-accommodation settings: Insights from the lacustrine valimi formation (gulf of Corinth, Greece). *Sedimentology* **2017**, *64*, 425–452.
9. Zhu, X.M.; Liu, Q.H.; Ge, J.W.; Dong, Y.L.; Zhu, S.F.; Tan, M.X.; Yang, Y. Reconstruction of sediment-dispersal patterns using seismic sedimentology in the southeastern Zhanhua Sag, Bohai Bay Basin, China. *J. Petro. Sci. Eng.* **2019**, *182*, 106335.
10. Hoy, R.G.; Ridgway, K.D. Sedimentology and sequence stratigraphy of fan-delta and river-delta deposystems, Pennsylvanian Minturn Formation, Colorado. *AAPG Bull.* **2003**, *87*, 1169–1191. [[CrossRef](#)]
11. Olariu, C.; Bhattacharya, J.P. Terminal distributary channels and delta front architecture of river-dominated delta systems. *J. Sediment. Res.* **2006**, *76*, 212–233. [[CrossRef](#)]
12. Winsemann, J.; Lang, J.; Fedele, J.J.; Zavala, C.; Hoyal, D.C. Re-examining models of shallow-water deltas: Insights from tank experiments and field examples. *Sediment. Geol.* **2021**, *421*, 105962. [[CrossRef](#)]
13. Xu, Z.H.; Björklund, P.P.; Wu, S.H.; Liu, Z.; Feng, W.J.; Zhang, K.; Yang, Z.; Zhong, Y.C. Sinuous bar fingers of digitate shallow-water deltas: Insights into their formative processes and deposits from integrating morphological and sedimentological studies with mathematical modelling. *Sedimentology* **2021**, *69*, 724–749. [[CrossRef](#)]
14. Zhang, J.Y.; Kim, W.; Olariu, C.; Steel, R. Accommodation-versus supply-dominated systems for sediment partitioning to deep water. *Geology* **2019**, *47*, 419–422. [[CrossRef](#)]
15. Qin, Y.; Zhu, X.M.; Zhu, S.F.; McElroy, B. Impact of deep-time palaeoclimate on the sedimentary records and morphology of lacustrine shoal-water deltas, Upper Eocene Dongying Depression, Bohai Bay Basin, China. *Sedimentology* **2021**, *68*, 3253–3278. [[CrossRef](#)]
16. Zou, C.N.; Zhang, X.Y.; Luo, P.; Wang, L.; Luo, Z.; Liu, L.H. Shallow-lacustrine sand-rich deltaic depositional cycles and sequence stratigraphy of the Upper Triassic Yanchang Formation, Ordos Basin, China. *Basin Res.* **2010**, *22*, 108–125.
17. Zhang, L.; Bao, Z.D.; Dou, L.X.; Zang, D.S.; Mao, S.W.; Song, J.; Zhao, J.H.; Wang, Z.C. 2018. Sedimentary characteristics and pattern of distributary channels in shallow water deltaic red bed succession: A case from the Late Cretaceous Yaojia formation, southern Songliao Basin, NE China. *J. Petrol. Sci. Eng.* **2018**, *171*, 1171–1190. [[CrossRef](#)]
18. Wang, M.Q.; Xie, J.; Zhang, Q.; Wang, Y.J.; Duan, Y.J. Characteristics and sedimentary model of a reticular shallow-water delta with distributary channels: Lower member of the Neogene Minghuazhen Formation in the Bozhong area of the Huanghekou Sag, China. *Arab. J. Geosci.* **2019**, *12*, 760. [[CrossRef](#)]
19. Olariu, C.; Zhou, C.M.; Steel, R.; Zhang, Z.J.; Yuan, X.J.; Zhang, J.Y.; Chen, S.; Cheng, D.W.; Kim, W. Controls on the stratal architecture of lacustrine delta successions in low-accommodation conditions. *Sedimentology* **2021**, *68*, 1941–1963. [[CrossRef](#)]
20. Wei, Z.D.; Li, S.L.; Zhang, T.; Liu, Y.; Yao, Z.Q.; Xu, W.Q.; Li, H. The delta-fluvial evolution of a lacustrine basin with gentle slope and low sedimentation rate: A case study of the Fudong Slope, Junggar Basin, Northwest China. *Sediment. Geol.* **2023**, *453*, 106441. [[CrossRef](#)]
21. Leeder, M.R.; Mack, G.H.; Salyards, S.L. Axial transverse fluvial interactions in half-graben: Plio-Pleistocene Palomas Basin, southern Rio Grande Rift, New Mexico, USA. *Basin Res.* **1996**, *8*, 225–241. [[CrossRef](#)]
22. Gawthorpe, R.L.; Leeder, M.R. Tectono-sedimentary evolution of active extensional basins. *Basin Res.* **2000**, *12*, 195–218. [[CrossRef](#)]
23. Ponte, F.C.; Fonseca, J.D.R.; Moralesa, R.G. Petroleum geology of eastern Brazilian continental margin. *AAPG Bull.* **1977**, *61*, 1470–1482.
24. Aloui, T.; Dasgupta, P.; Chaabani, F. Facies pattern of the Sidi Aïch formation: Reconstruction of Barremian paleogeography of Central North Africa. *J. Afr. Earth Sci.* **2012**, *71*, 18–42. [[CrossRef](#)]

25. Syvitski, J.P. Sediment fluxes and rates of sedimentation. In *Sedimentology*; Middleton, G., Church, M., Coniglio, M., Hardie, L., Longstaffe, F., Eds.; Springer: Berlin/Heidelberg, Germany, 1978; pp. 980–992.
26. Leeder, M.R.; Gawthorpe, R.L. Sedimentary models for extensional tilt-block/half-graben basins. *Geol. Soc. Lond. Spec. Publ.* **1987**, *28*, 139–152. [[CrossRef](#)]
27. Leeder, M.R.; Harris, T.; Kirkby, M.J. Sediment supply and climate change: Implications for basin stratigraphy. *Basin Res.* **1998**, *10*, 7–18. [[CrossRef](#)]
28. Dou, L.X.; Hou, J.G.; Liu, Y.M.; Zhang, L.; Song, S.H.; Wang, X.X. Sedimentary infill of shallow water deltaic sand bodies controlled by small-scale syndepositional faults related paleogeomorphology: Insights from the Paleogene Shahejie Formation in the Dongying Depression, Bohai Bay Basin, Eastern China. *Mar. Petrol. Geol.* **2020**, *118*, 104420. [[CrossRef](#)]
29. Zhu, H.T.; Yang, X.H.; Liu, K.Y.; Zhou, X. Seismic based sediment provenance analysis in continental lacustrine rift basins: An example from the Bohai Bay Basin, China. *AAPG Bull.* **2014**, *98*, 1995–2018. [[CrossRef](#)]
30. Wang, C.S.; Lin, C.S. Development status and trend of sedimentology in China in recent ten years. *Min. Miner. Pet. Petrol. Geochem. Bull.* **2021**, *40*, 1217–1229.
31. Zhang, D.Z.; Ji, Y.L.; Han, C.Y.; Lan, C.L.; Ni, C. Sedimentary characteristics and reservoir properties of the Shahejie Formation braided river delta in Raoyang Sag. *Geol. China* **2009**, *36*, 344–354. (In Chinese with English Abstract)
32. Du, W.; Li, K.; Ji, Y.L.; Lv, W.R.; Zhao, X.Y.; Huang, Z.J.; Jiang, Y.; Liu, Y.X.; Wang, Z.H.; Wu, H. A multi-stage expansion-to-regression model of Paleo-lakes in down-warp lacustrine basins. *Acta Sediment. Sin.* **2022**, *41*, 1097–1109. (In Chinese with English Abstract)
33. Yin, J.; Wang, Q.; Hao, F.; Guo, L.; Zou, H. Palaeoenvironmental reconstruction of lacustrine source rocks in the lower 1st Member of the Shahejie Formation in the Raoyang Sag and the Baxian Sag, Bohai Bay Basin, eastern China. *Palaeogeogr. Palaeoclima. Palaeoecol.* **2018**, *495*, 87–104. [[CrossRef](#)]
34. Ye, L.; Zhu, X.M.; Zhang, R.M.; Xie, S.H.; Gao, Y.; Tang, H.; Qi, X.Z.; Chen, Y.Q. Sedimentary environment of shallow-water delta and beach-bar of the Member 1 of Shahejie Formation in Lixian slope of Raoyang sag, Jizhong depression. *J. Paleo* **2020**, *22*, 587–600. (In Chinese with English Abstract)
35. Li, R.S. Characteristics of Provenance Analysis and Sedimentary Slope of Shahe Lixian County Street Group Sha Two Section to the Lower Part of Shahejie Formation. Master Dissertation, Southwest Petroleum University, Chengdu, China, 2012; pp. 13–44. (In Chinese with English Abstract)
36. Chen, H.H.; Zhu, X.M.; Wood, L.J.; Shi, R.S. Evolution of drainage, sediment-flux and fluvio-deltaic sedimentary systems response in hanging wall depocentres in evolving non-marine rift basins: Paleogene of Raoyang Sag, Bohai Bay Basin, China. *Basin Res.* **2019**, *32*, 116–145. [[CrossRef](#)]
37. Sun, D.S.; Liu, C.Y.; Yang, M.H.; Du, J.H.; Zhang, Y.M.; Zhang, R.F. Study on complex extensional structures in the middle Jizhong depression in the Bohai Bay Basin. *Geol. Rev.* **2004**, *50*, 484–491. (In Chinese with English Abstract)
38. Zhang, W.C.; Cui, Z.Q.; Han, C.Y.; Guo, Y.J.; Wang, H.S.; Li, L.; Wang, H.C.; Li, X.P. Evolution of Palaeogene lacustrine basins and oil and gas potentials in the central Hebei depression. *J. Paleo* **2001**, *3*, 45–54.
39. Posamentier, H.W.; Kolla, V. Seismic geomorphology and stratigraphy of depositional elements in deep-water settings. *J. Sediment. Res.* **2003**, *73*, 367–388. [[CrossRef](#)]
40. Wood, L.J. Quantitative seismic geomorphology of Pliocene and Miocene fluvial systems in the northern Gulf of Mexico, USA. *J. Sediment. Res.* **2007**, *77*, 713–730. [[CrossRef](#)]
41. Wood, L.J.; Mize-Spansky, K.L. Quantitative seismic geomorphology of a Quaternary leveed-channel system, offshore eastern Trinidad and Tobago, northeastern South America. *AAPG Bull.* **2009**, *93*, 101–125. [[CrossRef](#)]
42. Khan, H.A.; Qadir, S.A.; Khan, M.J.; Siddiqui, F.H.; Ahsan, M.S. Modelling of geomorphological features of fluvial systems in Eromanga Basin and North Sea using 3D seismic attributes. *J. Earth Sys. Sci.* **2023**, *132*, 62. [[CrossRef](#)]
43. Lerman, A.; Baccini, P. Lakes-chemistry, geology, physics. *J. Geol.* **1978**, *88*, 249–250.
44. Worash, G. Geochemistry provenance and tectonic setting of the Adigrat sandstone northern Ethiopia. *J. Afr. Earth Sci.* **2002**, *35*, 185–198.
45. Jin, Z.D.; Zhang, E.L. Paleoclimate implications of Rb/Sr ratios from lake sediments. *Sci. Technol. Eng.* **2002**, *2*, 20–22. (In Chinese with English Abstract)
46. Qian, H.J.; Lu, X.C.; Zhang, X.F.; Liu, Q. Spatial paleosalinity distribution and element geochemistry of argillaceous source rocks in the upper part of 4th Member of Tertiary Shahejie Formation in Dongying Sag. *Acta Petrologica Et Mineral.* **2009**, *28*, 161–168.
47. Bai, Y.; Liu, Z.; Sun, P.; Liu, R.; Hu, X.; Zhao, H.; Xu, Y. Rare earth and major element geochemistry of Eocene fine-grained sediments in oil shale- and coal-bearing layers of the Meihe Basin, northeast China. *J. Asian Earth Sci.* **2015**, *97*, 89–101. [[CrossRef](#)]
48. Herzsuh, U.; Zhang, C.; Mischke, S.; Herzsuh, R.; Mohammadi, F.; Mingram, B.; Kürschner, H.; Riedel, F. A late Quaternary lake record from the Qilian Mountains (NW China): Evolution of the primary production and the water depth reconstructed from macrofossil, pollen, biomarker, and isotope data. *Glob. Planet. Change* **2005**, *46*, 361–379. [[CrossRef](#)]

49. Mischke, S.; Herzschuh, U.; Zhang, C.; Bloemendal, J.; Riedel, F. A Late Quaternary lake record from the Qilian Mountains (NW China): Lake level and salinity changes inferred from sediment properties and ostracod assemblages. *Glob. Planet. Change* **2005**, *46*, 337–359. [[CrossRef](#)]
50. Frenzel, P.; Wrozyna, C.; Xie, M.; Zhu, L.; Schwalb, A. Palaeo-water depth estimation for a 600-year record from Nam Co (Tibet) using an ostracod-based transfer function. *Quat. Int.* **2010**, *218*, 157–165. [[CrossRef](#)]
51. Su, X.; Ding, X.; Jiang, Z.X.; Hu, B.; Meng, M.C.; Chen, M.S. Using of multi-microfossil proxies for reconstructing quantitative paleo-water depth during the deposit of LST of Es4s in Dongying Depression. *Earth Sci. Front.* **2012**, *19*, 188–199. (In Chinese with English Abstract)
52. Li, S.J.; Zheng, D.S.; Jiang, Z.X.; Hu, B.; Wang, J.X.; Jiao, Y.H. Water depth of paleo-lacustrine basin recovered by dominance diversity of Ostracoda: An example from sedimentary period of the Member 3 of Shahejie Formation of Paleogene in Dongying Sag, Shandong Province. *J. Palaeo* **2005**, *7*, 399–404. (In Chinese with English Abstract)
53. Jones, B.; Manning, D.A.C. Comparison of geochemical indices used for the interpretation of palaeoredox conditions in ancient mudstone. *Chem. Geol.* **1994**, *111*, 111–129. [[CrossRef](#)]
54. Wignall, P.B.; Twitchett, R.J. Oceanic anoxia and the end Permian mass extinction. *Science* **1996**, *272*, 1155–1158. [[CrossRef](#)] [[PubMed](#)]
55. Kimura, H.; Watanabe, Y. Ocean anoxia at the Precambrian-Cambrian boundary. *Geology* **2001**, *29*, 995–998. [[CrossRef](#)]
56. Bridge, J.S.; Mackey, S.D. A revised alluvial stratigraphy model. In *Alluvial Sedimentation*; Marzo, M., Puigdefabregas, C., Eds.; IAS Wiley: Oxford, UK, 1993; pp. 319–336.
57. Bridge, J.S.; Mackey, S.D. A theoretical study of fluvial sandstone body dimensions. In *Geological Modeling of Hydrocarbon Reservoirs*; Flint, S.S., Bryant, I.D., Eds.; IAS Wiley: Oxford, UK, 1993; pp. 213–236.
58. Bridge, J.S.; Tye, R.S. Interpreting the dimensions of ancient fluvial channel bars, channels, and channel belts from wireline-logs and cores. *AAPG Bull.* **2000**, *84*, 1205–1228.
59. Leclair, S.F.; Bridge, J.S. Quantitative interpretation of sedimentary structures formed by river dunes. *J. Sediment. Res.* **2001**, *71*, 713–716. [[CrossRef](#)]
60. Colomera, L.; Reesink, A.J.H.; Duller, R.A.; Jeavons, V.A.; Mountney, N.P. The thickness variability of fluvial cross-strata as a record of dune disequilibrium and palaeohydrology proxy: A test against channel deposits. *Sedimentology* **2024**, *71*, 590–618. [[CrossRef](#)]
61. Deng, Q.J.; Hu, M.Y.; Hu, Z.G. Depositional characteristics and evolution of the shallow water deltaic channel sand bodies in Fuyu oil layer of central downwarp zone of Songliao Basin, NE China. *Arab. J. Geosci.* **2019**, *12*, 607. [[CrossRef](#)]
62. Bristow, C.S. Brahmaputra River: Channel migration and deposition. In *Recent Developments in Fluvial Sedimentology*; Ethridge, F.G., Flores, R.M., Harvey, M.D., Eds.; SEPM Special Publication: Tulsa, Oklahoma, 1987; Volume 39, pp. 36–74.
63. Went, D.J. Fluvial shoal water deltas: Pre-vegetation sedimentation through the fluvial-marine transition, Lower Cambrian, English Channel region. *Sedimentology* **2020**, *67*, 330–363. [[CrossRef](#)]
64. Tye, R.S.; Coleman, J.M. Evolution of Atchafalaya lacustrine deltas, south-central Louisiana. *Sediment. Geol.* **1989**, *65*, 95–112. [[CrossRef](#)]
65. Went, D.J.; Hamilton, R.V.; Platt, N.H.; Underhill, J.R. Role of forced regression in controlling Brent Group reservoir architecture and prospectivity in the northern North Sea. *Pet. Geosci.* **2013**, *19*, 307–328. [[CrossRef](#)]
66. Fraser, G.S.; Hester, N.C. Sediments and sedimentary structures of a beach-ridge complex, southwestern shore of Lake Michigan. *J. Sediment. Res.* **1977**, *47*, 1187–1200.
67. Jiang, Z.X.; Liu, H.; Zhang, S.W.; Su, X.; Jiang, Z.L. Sedimentary characteristics of large-scale lacustrine beach-bars and their formation in the Eocene boxing sag of Bohai Bay Basin, east China. *Sedimentology* **2011**, *58*, 1087–1112. [[CrossRef](#)]
68. Galloway, W.E.; Hobday, D.K. Terrigenous shelf systems. In *Terrigenous Clastic Depositional Systems*; Springer: New York, NY, USA, 1996; pp. 159–185.
69. Martin, R. Paleogeomorphology and its application to exploration for oil and gas (with examples from western Canada). *AAPG Bull.* **1966**, *50*, 2277–2311.
70. Benson, J.D.; Pultz, L.M.; Bruner, D. The influence of paleotopography, sea level fluctuation, and carbonate productivity on deposition of the Smackover and Buckner formations, Appleton field, Escambia County, Alabama. *Gulf Coast Assoc. Geol. Soc. Trans.* **1996**, *46*, 15–23.
71. Clark, M.K. The significance of paleotopography. *Rev. Mineral. Geochem.* **2007**, *66*, 1–21. [[CrossRef](#)]
72. Allen, P.A. From landscapes into geological history. *Nature* **2008**, *451*, 274–276. [[CrossRef](#)]
73. Zeng, Z.W.; Zhu, H.T.; Mei, L.F.; Du, J.Y.; Zeng, H.L.; Xu, X.M.; Dong, X.Y. Multilevel source-to-sink (S2S) subdivision and application of an ancient uplift system in South China Sea: Implications for further hydrocarbon exploration. *J. Pet. Sci. Eng.* **2019**, *181*, 106220. [[CrossRef](#)]

74. Huang, C.Y.; Wang, H.; Zhang, H.W.; Wu, J.P.; Liu, Y.J. Oligocene shallow-water lacustrine deltas of the Baxian sag of Bohai Bay Basin, eastern China: Depositional response during rift-to-thermal tectonic subsidence transition. *AAPG Bull.* **2018**, *102*, 2389–2408. [[CrossRef](#)]
75. Candel, M.S. First record of *Palaeostomocystis subtilithecica* in Holocene marine sediments from the Beagle Channel, southern Tierra del Fuego, Argentina. *Rev. Palaeobot. Palynol.* **2015**, *221*, 52–58. [[CrossRef](#)]
76. Du, Q.X.; Guo, S.B.; Shen, X.L.; Cao, Z.H.; Zhang, X.L.; Li, Y.S. Palaeo-water characteristics of the Member 1 of Paleogene Shahejie Formation in southern Nanpu Sag, Bohai Bay Basin. *J. Palaeo* **2016**, *18*, 173–183. (In Chinese with English Abstract)
77. Cai, Q.S.; Hu, M.Y.; Liu, Y.N.; Kane, O.I.; Deng, Q.J.; Hu, Z.G.; Li, H.; Ngia, N.R. Sedimentary characteristics and implications for hydrocarbon exploration in a retrograding shallow-water delta: An example from the fourth member of the Cretaceous Quantou Formation in the Sanzhao depression, Songliao Basin, NE China. *Pet. Petrol. Sci.* **2022**, *2022*, 929–948. [[CrossRef](#)]
78. Dodd, J.R.; Stanton, R.J. *Paleoecology: Concepts and Application*; John Wiley Sons: New York, NY, USA, 1991.
79. Cronin, T.M.; Demartino, D.M.; Dwyer, G.S.; Rodriguez-Lazaro, J. Deep-sea ostracode species diversity: Response to late Quaternary climate change. *Mar. Micropaleontol.* **1999**, *37*, 231–249. [[CrossRef](#)]
80. Epstein, S.; Mayeda, T. Variation of O18 content of waters from natural sources. *Geochim. Cosmochim. Acta* **1953**, *4*, 213–224. [[CrossRef](#)]
81. Cao, H.; Guo, W.; Shan, X.; Ma, L.; Sun, P. Paleolimnological environments and organic accumulation of the Nenjiang Formation in the southeastern Songliao Basin, China. *Oil Shale* **2015**, *32*, 5–24. [[CrossRef](#)]
82. Moradi, A.V.; Sarı, A.; Akkaya, P. Geochemistry of the miocene oil shale (hançili formation) in the Çankırı-Çorum basin, central Turkey: Implications for paleoclimate conditions, source–area weathering, provenance and tectonic setting. *Sediment. Geol.* **2016**, *341*, 289–303. [[CrossRef](#)]
83. Wei, W.; Algeo, T.J. Elemental proxies for paleosalinity analysis of ancient shales and mudrocks. *Geochim. Cosmochim. Acta* **2020**, *287*, 341–366. [[CrossRef](#)]
84. Wignall, P.B.; Myers, K.J. Interpreting the benthic oxygen levels in mudrocks: A new approach. *Geology* **1988**, *16*, 452–455. [[CrossRef](#)]
85. Holden, C. Fossil trove preserved. *Science* **2001**, *291*, 1481.
86. Chen, Z.; Ding, Z.; Tang, Z.; Yang, S.; Wang, X.; Cui, L. Paleoweathering and paleoenvironmental change recorded in lacustrine sediments of the early to middle Eocene in Fushun Basin, Northeast China. *Geochem. Geophys. Geosyst* **2017**, *18*, 41–51. [[CrossRef](#)]
87. Wu, F.; Fang, X.; Herrmann, M.; Mosbrugger, V.; Miao, Y. Extended drought in the interior of Central Asia since the Pliocene reconstructed from sporopollen records. *Glob. Planet. Change* **2011**, *76*, 16–21. [[CrossRef](#)]
88. Miao, Y.; Fang, X.; Wu, F.; Cai, M.; Song, C.; Meng, Q.; Xu, L. Late Cenozoic continuous aridification in the western Qaidam Basin: Evidence from sporopollen records. *Clim. Past.* **2013**, *9*, 1863–1877. [[CrossRef](#)]
89. Sawyer, E.W. The influence of source rock type, chemical weathering and sorting on the geochemistry of clastic sediments from the Quetico metasedimentary belt, Superior Province. *Canada. Chem. Geol.* **1986**, *55*, 77–95. [[CrossRef](#)]
90. Bhattacharya, J.P.; Tye, R.S. Searching for modern Ferron analogs and application to subsurface interpretation. *Regional to wellbore analog for fluvial-deltaic reservoir modeling: The Ferron Sandstone of Utah: AAPG Stud. Geol.* **2004**, *50*, 39–57.
91. Bhattacharya, J.P.; Copeland, P.; Lawton, T.F.; Holbrook, J. Estimation of source area, river paleo-discharge, paleoslope, and sediment budgets of linked deep-time depositional systems and implications for hydrocarbon potential. *Earth Sci. Rev.* **2016**, *153*, 77–110. [[CrossRef](#)]
92. Postma, G. An Analysis of the Variation in Delta Architecture. *Terra Nova* **1990**, *2*, 124–130. [[CrossRef](#)]
93. Cleaves, E.T. Chemical weathering in a humid temperate environment. *Sci. Géologiques Bull. Et. Mémoires* **1983**, *72*, 47–55.
94. Shan, S.Q. Structural Geometry and Kinematics of the Taihang Mountain Piedmont Fault and Its Controlling on the Development of the Bohai Bay Basin. Ph.D. Dissertation, China University of Geosciences, Wuhan, China, 2018; p. 161.
95. Colombera, L.; Mountney, N.P. Scale dependency in quantifications of the avulsion frequency of coastal rivers. *Earth Sci. Rev.* **2022**, *230*, 104043. [[CrossRef](#)]
96. Cain, S.A.; Mountney, N.P. Spatial and temporal evolution of a terminal fluvial fan system: The Permian Organ Rock Formation, South-east Utah, USA. *Sedimentology* **2009**, *56*, 1774–1800. [[CrossRef](#)]
97. Van Der Kolk, D.A.; Flaig, P.P.; Hasiotis, S.T. Paleoenvironmental reconstruction of a late cretaceous, muddy, river-dominated polar deltaic system: Schrader bluff-prince Creek Formation transition, Shivugak bluffs, north slope of Alaska, USA. *J. Sediment. Res.* **2015**, *85*, 903–936. [[CrossRef](#)]
98. Aslan, A.; Autin, W.J.; Blum, M.D. Causes of river avulsion: Insights from the late Holocene avulsion history of the Mississippi River, USA. *J. Sediment. Res.* **2005**, *75*, 650–664. [[CrossRef](#)]
99. Stouthamer, E.; Cohen, K.M.; Gouw, M.J.P. Avulsion and its implications for fluvial-deltaic architecture: Insights from the Holocene Rhine-Meuse delta. In *From River to Rock Record: The Preservation of Fluvial Sediments and Their Subsequent Interpretation*; Davidson, S.K., Leleu, C.P., Eds.; SEPM Special Publication: Tulsa, Oklahoma, 2011; pp. 215–231.

100. Sahoo, H.; Gani, M.R.; Gani, N.D.; Hampson, G.J.; Howell, J.A.; Storms, J.E.A.; Martinius, A.W.; Buckley, S.J. Predictable patterns in stacking and distribution of channelized fluvial sand bodies linked to channel mobility and avulsion processes. *Geology* **2020**, *48*, 903–907. [[CrossRef](#)]
101. Ge, D.W. Forming Characteristics of Lithologic Reservoirs in Lixian Slope. Master's Dissertation, China University of Petroleum, Beijing, China, 2017; pp. 46–55. (In Chinese with English Abstract)
102. He, F.G.; Gao, X.Z.; Yang, D.X.; Fan, B.D.; Ren, C.Q.; Guo, H.P.; Wang, H.L.; Huang, Y.X. Controls on and geological models of hydrocarbon accumulation in gentle slopes caused by exceptionally weak tectonic activities: A case study of the Lixian Slope, Raoyang Sag, Eastern China. *Mar. Petro. Geol.* **2022**, *140*, 105661. [[CrossRef](#)]
103. Wei, Y.B. Regularity and Model of Shale Oil Enrichment in the Lower 1st Member of Shahejie Formation in Raoyang Sag, Jizhong Depression. Master's Dissertation, China University of Petroleum, Beijing, China, 2022; pp. 14–17. (In Chinese with English Abstract)

Disclaimer/Publisher's Note: The statements, opinions and data contained in all publications are solely those of the individual author(s) and contributor(s) and not of MDPI and/or the editor(s). MDPI and/or the editor(s) disclaim responsibility for any injury to people or property resulting from any ideas, methods, instructions or products referred to in the content.